Tuberculosis Exacerbates HIV-1 Infection through IL-10/STAT3-Dependent Tunneling Nanotube Formation in Macrophages

Shanti Souriant, Luciana Balboa, Maeva Dupont, Karine Pingris, Denise Kviatcovsky, Céline Cougoule, Claire Lastrucci, Aicha Bah, Romain Gasser, Renaud Poincloux, et al.

Article

Cell Reports

Tuberculosis Exacerbates HIV-1 Infection through IL-10/STAT3-Dependent Tunneling Nanotube Formation in Macrophages

Graphical Abstract

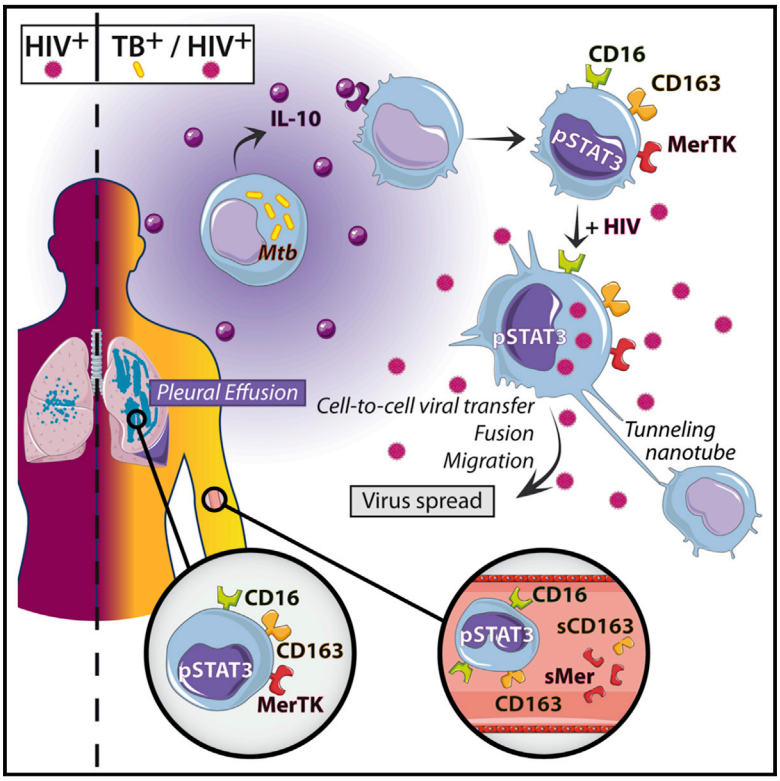

Highlights

- TB-induced anti-inflammatory M(IL-10) macrophages are prone to HIV-1 overproduction
- Tunneling nanotubes between TB-induced M(IL-10) macrophages promote HIV-1 spread
- The IL-10/STAT3 axis triggers tunneling nanotube induction in the TB microenvironment
- M(IL-10) macrophages accumulate in TB/HIV co-infected patients and non-human primates

Authors

Shanti Souriant, Luciana Balboa, Maeva Dupont, ..., Isabelle Maridonneau-Parini, Geanncarlo Lugo-Villarino, Christel Vérollet

Correspondence

lugo@ipbs.fr (G.L.-V.), verollet@ipbs.fr (C.V.)

In Brief

Tuberculosis is a clear, yet confounding, risk factor for HIV-1-induced morbidity and mortality. In this issue, Souriant et al. reveal that a tuberculosis-associated microenvironment triggers IL-10/STAT3-dependent tunneling nanotube formation in M(IL-10) macrophages, which promotes HIV-1 exacerbation during co-infection. M(IL-10) macrophage accumulation is also observed *in vivo* in co-infected subjects.

Souriant et al., 2019, Cell Reports *26*, 3586–3599
March 26, 2019
https://doi.org/10.1016/j.celrep.2019.02.091

CellPress

OPEN ACCESS
CellPress

Cell Reports
Article

Tuberculosis Exacerbates HIV-1 Infection through IL-10/STAT3-Dependent Tunneling Nanotube Formation in Macrophages

Shanti Souriant,[1,2] Luciana Balboa,[2,3] Maeva Dupont,[1,2] Karine Pingris,[1] Denise Kviatcovsky,[2,3] Céline Cougoule,[1,2] Claire Lastrucci,[1,4] Aicha Bah,[1] Romain Gasser,[5] Renaud Poincloux,[1] Brigitte Raynaud-Messina,[1] Talal Al Saati,[6] Sandra Inwentarz,[7] Susana Poggi,[7] Eduardo Jose Moraña,[7] Pablo González-Montaner,[7] Marcelo Corti,[8] Bernard Lagane,[5] Isabelle Vergne,[1] Carolina Allers,[9,10] Deepak Kaushal,[9,10] Marcelo J. Kuroda,[9,10,12] Maria del Carmen Sasiain,[2,3] Olivier Neyrolles,[1,2,11] Isabelle Maridonneau-Parini,[1,2,11] Geanncarlo Lugo-Villarino,[1,2,11,13,*] and Christel Vérollet[1,2,11,*]

[1]Institut de Pharmacologie et Biologie Structurale, IPBS, Université de Toulouse, CNRS, UPS, Toulouse, France
[2]International Associated Laboratory (LIA) CNRS "IM-TB/HIV" (1167), Toulouse, France, and Buenos Aires, Argentina
[3]Institute of Experimental Medicine–CONICET, National Academy of Medicine, Buenos Aires, Argentina
[4]Centre for Genomic Regulation, Barcelona, Spain
[5]Centre de Physiopathologie de Toulouse Purpan, INSERM UMR 1043, CNRS UMR 5282, Université Toulouse III Paul Sabatier, Toulouse, France
[6]INSERM/UPS/ENVT–US006/CREFRE, Service d'Histopathologie, CHU Purpan, 31024 Toulouse, France
[7]Instituto de Tisioneumonologia "Raúl F. Vaccarezza," Universitad de Buenos Aires, Argentina
[8]Division de SIDA, Hospital de Infecciosas Dr. F.J. Muñiz, Buenos Aires, Argentina
[9]Tulane National Primate Research Center, Covington, LA 70433, USA
[10]Department of Microbiology and Immunology, School of Medicine, Tulane University, New Orleans, LA 70112, USA
[11]These authors contributed equally
[12]Present address: Center for Comparative Medicine and California National Primate Research Center, University of California, Davis, Davis, CA 95616, USA
[13]Lead Contact
*Correspondence: lugo@ipbs.fr (G.L.-V.), verollet@ipbs.fr (C.V.)
https://doi.org/10.1016/j.celrep.2019.02.091

SUMMARY

The tuberculosis (TB) bacillus, *Mycobacterium tuberculosis* (Mtb), and HIV-1 act synergistically; however, the mechanisms by which Mtb exacerbates HIV-1 pathogenesis are not well known. Using *in vitro* and *ex vivo* cell culture systems, we show that human M(IL-10) anti-inflammatory macrophages, present in TB-associated microenvironment, produce high levels of HIV-1. *In vivo*, M(IL-10) macrophages are expanded in lungs of co-infected non-human primates, which correlates with disease severity. Furthermore, HIV-1/Mtb co-infected patients display an accumulation of M(IL-10) macrophage markers (soluble CD163 and MerTK). These M(IL-10) macrophages form direct cell-to-cell bridges, which we identified as tunneling nanotubes (TNTs) involved in viral transfer. TNT formation requires the IL-10/STAT3 signaling pathway, and targeted inhibition of TNTs substantially reduces the enhancement of HIV-1 cell-to-cell transfer and overproduction in M(IL-10) macrophages. Our study reveals that TNTs facilitate viral transfer and amplification, thereby promoting TNT formation as a mechanism to be explored in TB/AIDS potential therapeutics.

INTRODUCTION

Worldwide, individuals co-infected with *Mycobacterium tuberculosis* (Mtb), the agent of tuberculosis (TB), and the AIDS virus, HIV-1, pose particular clinical challenges not only because a significant proportion of co-infected patients remain sputum smear-negative, hampering TB diagnosis, but also because HIV-1 infection makes these individuals more prone to TB reactivation (World Health Organization [WHO] TB 2016, Joint United Nations Programme on HIV and AIDS [UNAIDS] Report 2016) (Getahun et al., 2007). At the heart of this problem is the synergy between HIV-1 and Mtb, which interferes with treatment and promotes the pathogenesis of both pathogens (Diedrich and Flynn, 2011; Diedrich et al., 2016). On the one hand, $CD4^+$ T cell decay and other mechanisms induced by HIV-1 are a leading cause for reactivation of latent TB and progression to active TB disease in AIDS patients (Bell and Noursadeghi, 2018; Tomlinson et al., 2013). On the other hand, clinical and epidemiological data clearly identify TB as a risk factor amplifying HIV-1-associated morbidity and mortality (Toossi, 2003). However, the mechanisms by which Mtb exacerbates HIV-1 infection require further investigation (Charles and Shellito, 2016; Esmail et al., 2018; Toossi, 2003; Bell and Noursadeghi, 2018). Addressing this issue should help in developing strategies for the attenuation of viral activation in co-infected subjects and for a better control of the AIDS epidemic (Diedrich and Flynn, 2011).

Lung macrophages are the primary host cells for Mtb (O'Garra et al., 2013; Russell et al., 2010). While $CD4^+$ T cells are the major target cells for HIV-1, macrophages, including those in the lungs, are also infected by HIV-1 in humans (Bell and Noursadeghi, 2018; Cribbs et al., 2015) and by simian immunodeficiency virus (SIV) in experimentally infected non-human primates (NHPs) (Avalos et al., 2016). Recent data indicate that macrophages play an important role in HIV-1 pathogenesis (Honeycutt et al., 2016, 2017; Sattentau and Stevenson, 2016) and may also be involved in HIV-1/Mtb co-infection (Khan and Divangahi, 2018; Kuroda et al., 2018). In HIV-1-infected individuals with active TB, for example, macrophages from the lungs and pleural effusions (PEs) exhibit high levels of HIV-1 infection (Lawn et al., 2001; Toossi, 2003). Furthermore, Mtb increases the level of HIV-1 infection either *in vitro* in monocyte-derived macrophages or *ex vivo* in lung macrophages obtained from patients with HIV-1 (Mancino et al., 1997; Toossi et al., 1997). It is presently unclear how a TB-associated microenvironment renders macrophages more susceptible to HIV-1.

Macrophages display considerable heterogeneity in tissues (Gordon et al., 2014). The broad spectrum of pro- (M1) and anti-inflammatory (M2) activation programs are a manifestation of the different levels of response to HIV-1 and Mtb infections (Cassol et al., 2009; Lugo-Villarino et al., 2011). We have shown that active TB skews human monocyte differentiation toward M2-like macrophages, distinguished by a $CD16^+CD163^+MerTK^+$ phenotype, as well as by increased immunomodulatory activity and Mtb permissivity (Lastrucci et al., 2015). This phenotype is dependent on the interleukin-10 (IL-10)/STAT3 signaling axis and is closely related to the so-called "M(IL-10)" activation program (Murray et al., 2014). We further reported that the abundance of M(IL-10) cells correlates with TB severity in patients and NHPs (Lastrucci et al., 2015). Herein, we investigated whether the TB-induced M(IL-10) macrophage activation program also plays a role in promoting HIV-1 infection in co-infected individuals.

RESULTS

TB-Associated Microenvironment Increases HIV-1 Infection in Human Macrophages

To determine whether HIV-1 replication is modulated in TB-induced M(IL-10) macrophages, we employed our previously described *in vitro* model (Lastrucci et al., 2015), which uses conditioned medium from either mock-infected macrophages (CmCTR) or Mtb-infected macrophages (CmMTB). CmMTB triggered primary human monocytes to differentiate into M(IL-10) macrophages, which activated STAT3, as well as acquired a $CD16^+CD163^+MerTK^+PD\text{-}L1^+$ receptor signature, similar to differentiated M(IL-10) macrophages observed *in vivo* (Figure S1; Lastrucci et al., 2015). When macrophages treated with either CmCTR or CmMTB were then infected with HIV-1 ADA (Figure 1A) or NLAD8 strain (data not shown) (Raynaud-Messina et al., 2018), we observed a substantial increase in viral replication, as measured by the level of the viral protein p24 in culture supernatants, only in the CmMTB-treated M(IL-10) macrophages (Figures 1B and S2A). In addition, the number of HIV-1-infected cells increased by 3-fold, as measured by the expression of the HIV-1 Gag protein (Figures 1C and 1D). The M(IL-10) receptor signature was maintained upon HIV-1 infection (Figure S1). HIV-1 infection of macrophages enhanced their migration capacity in dense 3-dimensional matrices, together with their fusion potential, forming multinucleated giant cells (MGCs) (Orenstein, 2000; Vérollet et al., 2010, 2015a). We found that these properties, known to contribute to viral dissemination (Vérollet et al., 2015a, 2015b), were further amplified specifically in M(IL-10) macrophages infected with HIV-1 (Figures S2B–S2E).

PE fluid from TB patients (PE-TB) was used as an *ex vivo* TB-associated microenvironment model (Genoula et al., 2018). PE is observed in up to 30% of TB patients and results from infection-induced local inflammation and recruitment of leukocytes into the pleural space (Vorster et al., 2015). In co-infected patients, the formation of PE is more common than in TB patients and PE contains high viral titers, compared to serum from the same patient (Collins et al., 2002; Toossi, 2003). Unlike control PE obtained from non-TB patients (PE-non-TB), differentiation of macrophages in the presence of PE-TB (Table S1; Figure 1A) yielded the M(IL-10) phenotype (Figures S3A and S3B), similar to macrophages isolated from PE-TB (Lastrucci et al., 2015). This M(IL-10) phenotype also correlated with the high level of soluble IL-10 contained in PE-TB compared to PE-non-TB (Figure S3C). We found that cell treatment with PE-TB increased the production of HIV-1 by 6-fold and increased the number of infected macrophages and MGCs (Figures 1E–1G and S3D).

Collectively, using CmMTB- and PE-TB-conditioned macrophages as model systems, we show that HIV-1 production by M(IL-10) macrophages is enhanced in a TB-associated microenvironment.

M(IL-10) Cells Accumulate in Co-infected NHPs and Patients

To investigate M(IL-10) cells in HIV-1/Mtb co-infections, we compared, by using CD163 and pSTAT3 staining (Lastrucci et al., 2015), the number of M(IL-10) macrophages in pulmonary samples from NHPs that had been (1) co-infected with Mtb (active or latent TB) and SIV; (2) mono-infected with Mtb (active or latent TB); (3) mono-infected with SIV (Cai et al., 2015; Kuroda et al., 2018); or (4) uninfected (Tables S2 and S3). Histological staining revealed abundant $CD163^+$ and nuclear $pSTAT3^+$ cells in co-infected NHPs (Figures 2A and 2B). While the detection of pSTAT3 is not specific to macrophages, double-staining analysis demonstrated that most $CD163^+$ alveolar macrophages were also positive for nuclear pSTAT3 (Figure 2C). The increased abundance of $CD163^+$ and $pSTAT3^+$ cells was correlated with the severity of lung histopathology (Table S3) and the gross pathological status of the animals, as analyzed in 30 organs (Figures 2D and 2E).

We have previously shown that $CD14^+CD16^+$ circulating monocytes have a predisposition to differentiate into M(IL-10) macrophages in patients with active TB (Lastrucci et al., 2015). Here, we confirmed that $CD14^+CD16^+$ monocytes are expanded in the peripheral blood of TB, HIV-1, and co-infected patients, compared to healthy subjects (Balboa et al., 2011; Ellery et al., 2007; Ziegler-Heitbrock, 2007) (Table S1; Figure S4A). We examined two cell surface markers characteristic of the M(IL-10) phenotype, which are selectively expressed in the monocytic lineage, CD163 and MerTK, and which are both subjected to inflammation-driven shedding (Fabriek et al., 2005; Sather

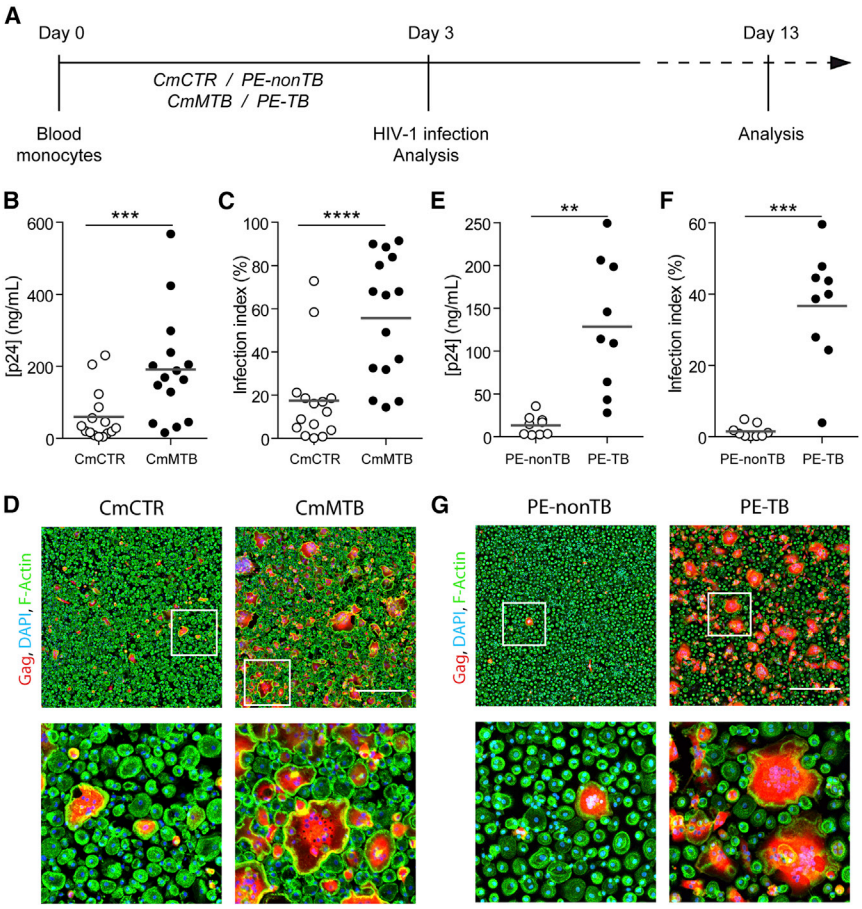

Figure 1. TB-Induced Microenvironment Exacerbates HIV-1 Infection of M(IL-10) Macrophages

(A) Representation of the experimental design of two *in vitro* models. Briefly, monocytes from healthy subjects were treated either with conditioned medium from mock-infected (CmCTR) or Mtb-infected macrophages (CmMTB), or with pleural effusions (PEs) from TB (PE-TB) or non-TB (PE-nonTB) patients for 3 days. Cells were then infected with HIV-1 ADA strain at MOI of 0.1 and kept in culture for at least 10 more days.

(B) Vertical scatterplot showing p24 concentration from day 13 supernatants of HIV-1-infected macrophages treated with CmCTR or CmMTB.

(C) Vertical scatterplot showing the infection index of day 13 HIV-1-infected macrophages treated with CmCTR or CmMTB. Infection index was calculated as 100 × the ratio of the area covered by Gag^+ cells over the total cell area, measured from immunofluorescence (IF) images.

(D) Representative IF images of day 13 HIV-1-infected macrophages treated with CmCTR or CmMTB. HIV-1 Gag (red), F-actin (green), and DAPI (blue). Scale bar, 500 μm. Insets are 4× zooms (lower panels).

(E) Vertical scatterplot showing p24 concentration from day 13 supernatants of HIV-1-infected macrophages treated with PE-TB or PE-nonTB.

(F) Vertical scatterplot showing the infection index of day 13 HIV-1-infected macrophages treated with PE-TB or PE-nonTB.

(G) Representative IF images of day 13 HIV-1-infected macrophages treated with PE-nonTB or PE-TB. HIV-1 Gag (red), F-actin (green), and DAPI (blue). Scale bar, 500 μm. Insets are 4× zooms (lower panels). Each circle within vertical scatterplots represents a single donor. Mean value is represented as a dark gray line.

In this figure, PE-nonTB are parapneumonic PE. Statistical analyses: two-tailed, Wilcoxon matched-paired signed rank test (B and C); paired t test (E and F). $^{**}p \leq 0.005$; $^{***}p \leq 0.0005$; $^{****}p \leq 0.0001$. See also Figures S1–S3.

et al., 2007). We found that the soluble forms of these receptors (sCD163 and sMer), but not their membrane-bound forms, were substantially increased in co-infected patients when compared to mono-infected patients and healthy subjects (Figure 3). The amount of these soluble factors correlated with one another (Figure S4B). Receiver operating characteristic (ROC) curve analyses for plasma concentration of sCD163 and sMer (Figures S4C and S4D) suggested both molecules may be useful biomarkers for co-infection.

Our findings reveal the extent of the *in vivo* expansion of TB-induced M(IL-10) cell population in co-infected individuals. They also identify potential biomarkers for diagnosis and monitoring TB in co-infected patients.

TB-Associated Microenvironments Enhance Tunneling Nanotube Formation

TB-associated microenvironment could increase the level of HIV-1 in M(IL-10) macrophages by modulating viral (1) entry, (2) replication, (3) clearance, (4) infectivity of the produced virions, and/or (5) cell-to-cell transmission. We tested each of these possibilities in turn. Although cell-surface expression of the HIV-1 entry receptors CD4, CCR5, and CXCR4 was increased in CmMTB-treated cells compared to control cells (Figure 4A), virus entry was unchanged in these cells, as shown using the BlaM-Vpr fusion assay (Cavrois et al., 2002) (Figure 4B). The expression level of several host factors known to be involved in HIV-1 replication (CEBP-β and CUGBP1) or restriction (IFITM proteins and SAMHD1) was not modified by CmMTB (Figures 4C–4F). As autophagy represents a viral clearance mechanism known to be inhibited by HIV-1 or Mtb infection in macrophages (Espert et al., 2015), we measured the autophagic flux and found it to be similar between CmMTB- and CmCTR-treated cells (Figure 4G). Furthermore, the infectivity of viruses produced in CmMTB conditions was comparable to those produced in CmCTR-treated cells (7.7% ± 2.1% of p24-positive TZM-bl [Vérollet et al., 2015a] for CmMTB-treated macrophages versus 10.3% ± 3.5% for CmCTR-treated cells; n = 3; p = 0.5066).

Finally, we investigated whether cell-to-cell virus transfer was influenced by TB-associated microenvironment. Tunneling nanotube (TNT) formation has been proposed as a macrophage-to-macrophage transmission process for host and microbial material (Dupont et al., 2018; Eugenin et al., 2009; Hashimoto et al., 2016; Okafo et al., 2017). Importantly, TNT formation is triggered by HIV-1 infection of macrophages and it has been associated with

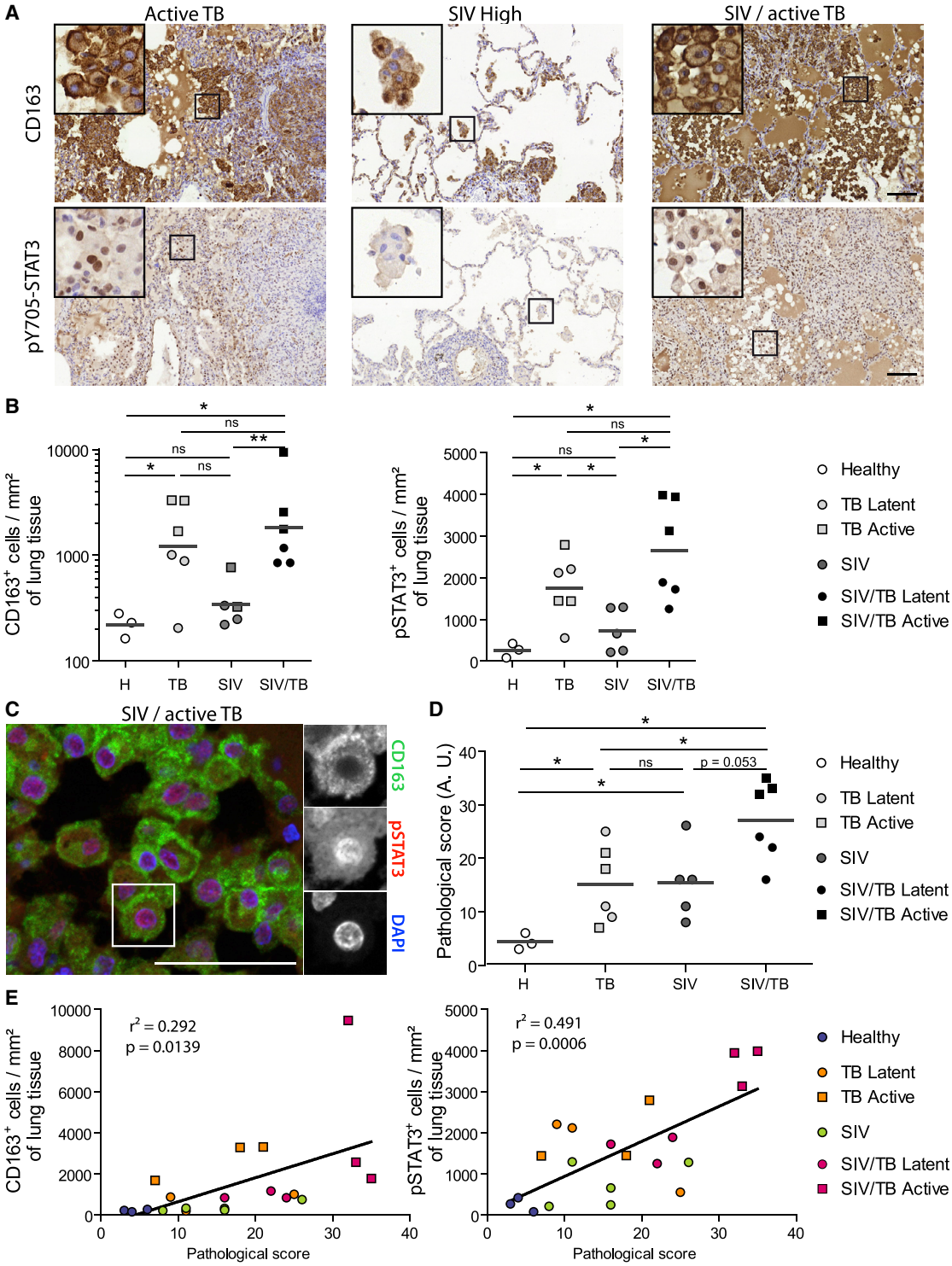

Figure 2. Accumulation of M(IL-10) Macrophages in the Lung of Co-infected NHPs Correlates with Pathology

(A) Representative immunohistochemical images illustrate higher number of CD163$^+$ cells and p-STAT3$^+$ cells in lung biopsies of SIV-Mtb-infected NHPs compared to Mtb or SIV mono-infected NHPs. Scale bar, 100 μm. Insets are 4× zooms.

(B) Quantification of the number of CD163$^+$ cells (left) and p-STAT3$^+$ cells (right) per square millimeter of lung tissue of healthy (H), SIV-infected, Mtb-infected, and SIV-Mtb-co-infected NHPs.

(C) Immunohistochemistry staining of lung biopsy of SIV-Mtb co-infected NHP showing the nuclear localization of p-STAT3 (red, center) in CD163 alveolar macrophages (green, top). Nuclei are stained using DAPI (blue, bottom). Scale bar, 50 μm. Insets are 1.3× zooms.

(legend continued on next page)

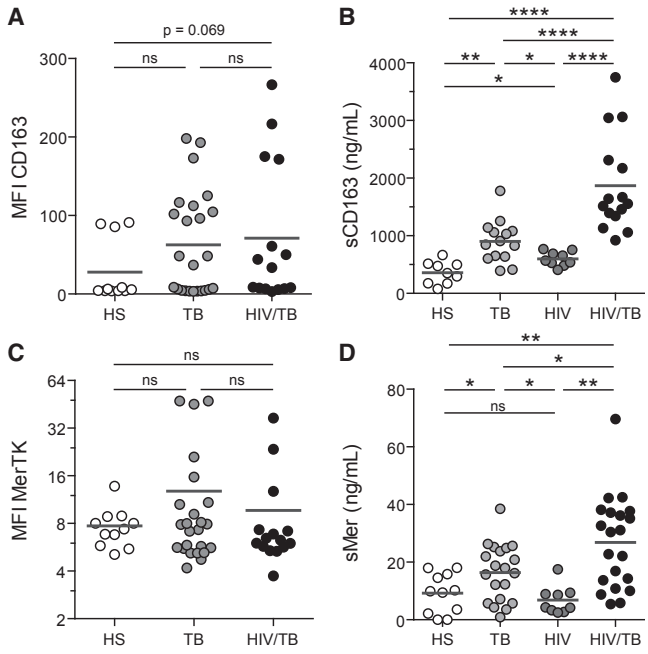

Figure 3. Systemic Expansion of the M(IL-10) Monocyte Population in Co-infected Patients

(A) Vertical scatterplots showing the median fluorescence intensity (MFI) of cell-surface marker CD163 on $CD14^+$ monocytes from peripheral blood (PB) of healthy subjects, TB patients (TB), and HIV/Mtb co-infected patients (HIV/TB).

(B) Vertical scatterplots showing the amount of sCD163, the cleaved form of CD163 in the serum of healthy subjects and TB, HIV, and HIV/TB patients.

(C) Vertical scatterplots showing the MFI of cell-surface marker MerTK on $CD14^+$ monocytes from PB of healthy subjects and TB and HIV/TB patients.

(D) Vertical scatterplots showing the amount of sMer, the cleaved form of MerTK, in the serum of healthy subjects and TB, HIV, and HIV/TB patients. Each circle within vertical scatterplots represents a single donor. Mean value is represented as a dark gray line.

Statistical analyses: two-tailed, Mann-Whitney (A–C); unpaired t test (D). $^*p \leq 0.05$; $^{**}p \leq 0.005$; $^{***}p \leq 0.0005$; ns, not significant. See also Figure S4 and Table S1.

an increase in viral replication (Eugenin et al., 2009; Hashimoto et al., 2016). TNTs are long-range membranous F-actin-containing tubes, not in contact with the extracellular substrate, which are classified into two types based on their thickness and on whether they contain microtubules (Ariazi et al., 2017; Dupont et al., 2018; McCoy-Simandle et al., 2016; Onfelt et al., 2006) (Figure 5A). Treatment with CmMTB increased the percentage of cells forming both types of TNTs by more than 2-fold (Figures 5A and 5B), compared to CmCTR-treated cells, and HIV-1 infection further amplified this phenomenon (Figures 5B and 5C).

Using different microscopy approaches, we further characterized TNTs in macrophages as induced by TB-associated microenvironment. TNTs are (1) long (up to 200 μm in length), actin-containing structures connecting two cells, which are above the surface of the substrate (Figures 5D, S5A, and S5B; Videos S1 and S2) (Dupont et al., 2018); (2) positive for M-Sec, a regulator of TNT formation (Hase et al., 2009) (Figure S5C; Video S4); and (3) inhibited by cytochalasin D treatment (39% ± 5% of TNTs in HIV-1-infected CmMTB-treated macrophages versus 6% ± 4% upon 2 μM Cytochalasin D treatment; n = 3; p = 0.0003). We also observed that CmMTB-induced TNTs contained HIV-1 material and particles (Figures 5E and 5F; Video S3). Of note, we detected putative TNT-like structures in pulmonary samples from NHPs co-infected with Mtb and SIV, as revealed by H&E staining, or by immunohistochemistry targeting CD163-positive macrophages (Figure S5D).

Taken together, these data indicate that TB-associated microenvironments do not affect the entry, replication, or turnover of HIV-1. Instead, they trigger the formation of TNTs in M(IL-10) macrophages that appear to contain HIV-1 particles.

IL-10/STAT3 Promotes TNTs and Increased Viral Production in Macrophages

We have previously reported that the expansion of M(IL-10) macrophages relies on the IL-10/STAT3 signaling pathway (Lastrucci et al., 2015). To study how TB-associated microenvironment triggers the formation of TNTs in macrophages, we examined whether IL-10/STAT3 signaling was required for TNT formation and increased HIV-1 production induced by TB-associated microenvironment. Recombinant IL-10 triggered M(IL-10) macrophage differentiation (Lastrucci et al., 2015) (Figure S6A), increased TNT formation (Figure 6A) and recapitulated the TB-driven expansion of HIV-1 infection, as measured by p24 release, number of infected cells (Figure 6B), and formation of MGCs (Figure S6B). Depletion of IL-10 from CmMTB abolished enhanced TNT formation, the increase in HIV-1 replication in M(IL-10) cells, and the increase in MGCs (Figures 6C, 6D, and S6C). We examined the role of STAT3 activation by pharmacological inhibition with Stattic, which targets the STAT3 SH2 domain to prevent association with upstream kinases and abrogates STAT3 phosphorylation and the associated M(IL-10) phenotype (Lastrucci et al., 2015). Stattic treatment inhibited both the CmMTB-driven TNT formation and the increase in HIV-1 production (Figures 6E and 6F), along with enhanced cell migration and formation of MGCs (Figures S2E and S6D). Of note, treatment of monocytes with other cytokines prior to HIV-1 infection does not trigger TNT formation significantly, indicating that IL-10 is one of the main factor involved in this process (Figure S6E).

Our data demonstrate that TB-associated microenvironment controls TNT formation and increase HIV-1 infection in macrophages. In addition, they reveal the IL-10/STAT3 axis as a signaling pathway involved in TNT formation.

(D) Vertical scatterplot showing the pathological scoring of NHPs used in this study (see Table S3).

(E) Correlation between $CD163^+$ cells (left) or p-$STAT3^+$ cells (right) per square millimeter of lung tissue and pathological score in the indicated NHPs. Each symbol within vertical scatterplots represents a single animal. Mean value is represented as a dark gray line.

Statistical analyses: two-tailed Mann-Whitney (B and D). $^*p \leq 0.05$; $^{**}p \leq 0.005$; ns, not significant. See also Tables S2 and S3.

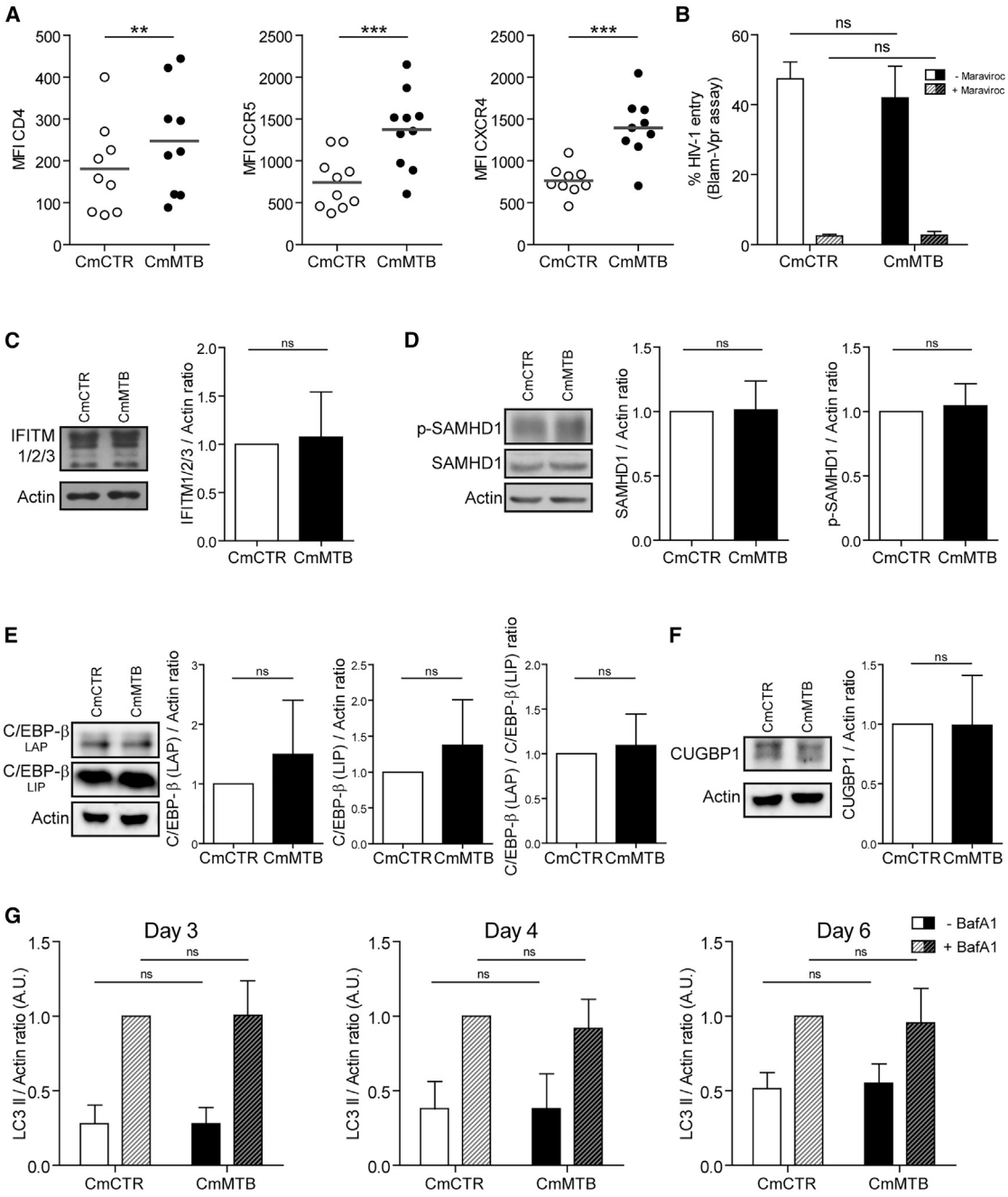

Figure 4. The TB-Driven Exacerbation of HIV-1 Infection in Macrophages Is Not Due to Modulation in Viral Entry, HIV-1-Related Activation or Restriction Factors, or Autophagy

(A) Vertical scatterplots showing the median fluorescence intensity (MFI) of cell-surface receptors involved in HIV-1 entry (CD4, CCR5, CXCR4) on monocytes differentiated for 3 days under the presence of CmCTR and CmMTB. Each circle within vertical scatterplots represents a single donor. Mean value is represented as a dark gray line.

(B) Histogram showing the percentage of HIV-1 fusion with CmCTR (white)- or CmMTB (black)-pre-treated cells, as determined using the Blam-Vpr assay in the presence of entry inhibitor Maraviroc (dashed bars).

(C) Left: representative images of western blot analysis illustrating the expression of IFITM1/2/3 and Actin as loading control. Right: quantification of IFITM1/2/3 expressed as a ratio related to actin of monocytes differentiated for 3 days into macrophages under the presence of CmCTR (white) and CmMTB (black). n = 6 donors.

(D) Representative images of western blot analysis illustrating the expression of SAMHD1 and its phosphorylated version (pSAMHD1), and Actin as loading control (left). Quantification of SAMHD1 (center) pSAMHD1 (right) expressed as a ratio related to actin of monocytes differentiated for 3 days into macrophages under the presence of CmCTR and CmMTB. n = 11 donors.

(legend continued on next page)

TNTs Participate in the High Viral Production in M(IL-10) Macrophages

To determine whether TNT formation is involved in the increased HIV-1 production in M(IL-10) macrophages, we used a previously described pharmacological inhibitor of TNT formation, TNTi (Hashimoto et al., 2016). We observed that TNTi inhibited the TNT-mediated transfer of fluorescent material between Di0-stained cells and CellTracker-positive cells (Figure S7A), without affecting macrophage viability, or F-actin-dependent processes like podosome formation and phagocytosis (Maridonneau-Parini, 2014) (Figures S7B–S7E). In TB-induced M(IL-10) macrophages infected with HIV-1, TNTi strongly inhibited TNT formation (Figure 7A), significantly diminished HIV-1 overproduction (Figure 7B), and reduced MGC formation (Figure S7F).

Unlike in T lymphocytes, the transfer of HIV-1 particles via TNTs has been suggested but not formally demonstrated in macrophages (Dupont et al., 2018; Eugenin et al., 2009; Hashimoto et al., 2016; Okafo et al., 2017). Thus, we set up a co-culture system between M(IL-10) macrophages to assess the transfer of the viral Gag protein from infected donor cells to uninfected recipient cells. Uninfected (recipient, CellTracker$^+$, green) and HIV-1-infected (donor, Gag$^+$, red) macrophages were either co-cultured or separated by a transwell membrane that blocks cell-to-cell connections (Figure 7C). Importantly, TNT quantification showed that productively infected macrophages preferentially formed TNT (38% ± 6% of TNT formation in Gag$^+$ cells compared to 21% ± 7% in non-infected CellTracker$^+$ cells; n = 5; p = 0.0003). After 24 h in co-culture, we observed that donor macrophages were able to transfer the virus to recipient macrophages, which became HIV-1 positive (Figure 7D; Videos S5 and S6). By contrast, the transfer of HIV-1 from donor to recipient macrophages was blocked in the transwell cultures (Figure 7E), showing that cell-to-cell contacts are involved in this process. In co-culture experiments, TNTi significantly diminished the capacity of M(IL-10) macrophages to transfer HIV-1 to recipient cells (Figure 7E), indicating that TNT formation is responsible for cell-to-cell viral spread.

These results establish a role for TNTs in spreading the virus between M(IL-10) macrophages, uncovering a key cellular mechanism responsible for HIV-1 overproduction in the context of TB.

DISCUSSION

TB is the most common co-infection among people living with HIV-1 and is a leading cause of AIDS-related deaths. Here, we asked whether TB-associated microenvironment influences the control of HIV-1 infection in human macrophages. We report that M(IL-10) macrophages (CD163$^+$MerTK$^+$CD16$^+$pSTAT3$^+$), which accumulate in TB patients and can be derived *in vitro* from TB-associated microenvironment, are highly permissive for HIV-1 production. This exacerbation of HIV-1 infection involves the IL-10/STAT3 signaling axis, which controls TNT formation, thus enhancing cell-to-cell transfer of the virus in our experimental systems. *In vivo*, M(IL-10) cells are more abundant in co-infected individuals compared to mono-infection settings. We have identified potential biomarkers, sCD163 and sMer, in the blood of co-infected patients, which could be used to monitor disease progression, as their expression correlates with the severity of the pathology. All things considered, our study makes three important contributions to the general understanding of how TB exacerbates HIV-1 infection.

First, we show that M(IL-10) macrophages (CD163$^+$pSTAT3$^+$) accumulate in co-infected patients and NHPs. In co-infected NHPs, we observe M(IL-10) macrophages in great abundance in the lung environment, including the alveolar space and the lung interstitial tissue. M(IL-10) macrophage abundance in lungs is correlated with the pathological score of the animals, arguing for the physiological and pathological pertinence of these macrophages. These macrophages are likely driven by the IL-10/STAT-3 signaling pathway and originate from CD14$^+$CD16$^+$ monocytes (Lastrucci et al., 2015), which are increased in the blood of patients with active TB, regardless of their HIV-1 infection status (Ziegler-Heitbrock, 2007). Monocytes are the only circulating leukocytes known to express membrane-bound CD163 and MerTK (Fabriek et al., 2005; Sather et al., 2007). As these membrane receptors are subjected to inflammation-driven shedding (Fabriek et al., 2005; Sather et al., 2007), their soluble form in the blood can be used as a proxy for estimating the abundance of CD14$^+$CD16$^+$ monocytes in the circulation. Here, we show that, in HIV-1$^+$ patients with active TB, the plasma levels of both sCD163 and sMer are significantly higher than those found in healthy subjects, HIV-1- or Mtb-infected patients. sCD163 is already described as a clinical indicator of monocyte activation in HIV-1 patients (Burdo et al., 2011), as an indicator of lesions and accumulation of macrophages in the brain of SIV-infected NHPs (Burdo et al., 2010), and as an independent predictor of survival in TB (Knudsen et al., 2005). Although our findings will need to be expanded in larger cohorts, they nevertheless reveal both sCD163 and sMer as potential tools for the diagnosis and disease monitoring in HIV-1/Mtb co-infected patients. Because TB diagnosis in HIV-1-infected individuals remains a major

(E) Representative images of western blot analysis illustrating the expression of C/EBP-β (LAP), C/EBP-β (LIP), and Actin as loading control (left). Quantification of C/EBP-β (LAP, center left) and C/EBP-β (LIP, center right) expressed as a ratio related to actin, and LAP expressed as a ratio related to LIP (right), of monocytes differentiated for 3 days into macrophages under the presence of CmCTR and CmMTB. n = 9 donors. LAP is an activator of HIV-1-LTR, whereas LIP is a repressor of HIV-1-LTR.

(F) Representative images of western blot analysis illustrating the expression of CUGBP1 and Actin as loading control (left). Quantification of CUGBP1 expressed as a ratio related to actin (right) of monocytes differentiated for 3 days into macrophages under the presence of CmCTR and CmMTB. n = 9 donors.

(G) Quantification of LC3-II expression as a ratio to actin of monocytes differentiated for 3 days under the presence of CmCTR and CmMTB at the indicated time points after 2 h treatment with Bafilomycin A1 (BafA1) or DMSO as control, as measured by western blot analysis. Uninfected cells at day 3 of the experiment (left; n = 6 donors), and HIV-infected cells at 1 (day 4; center; n = 4 donors) and 3 (day 6; right; n = 6 donors) days post-infection. Each circle within vertical scatterplots represents a single donor. Mean value is represented as a dark gray line.

Data in histograms are represented as mean ± SD. *p ≤ 0.05; **p ≤ 0.005; ***p ≤ 0.0005; ****p ≤ 0.0001.

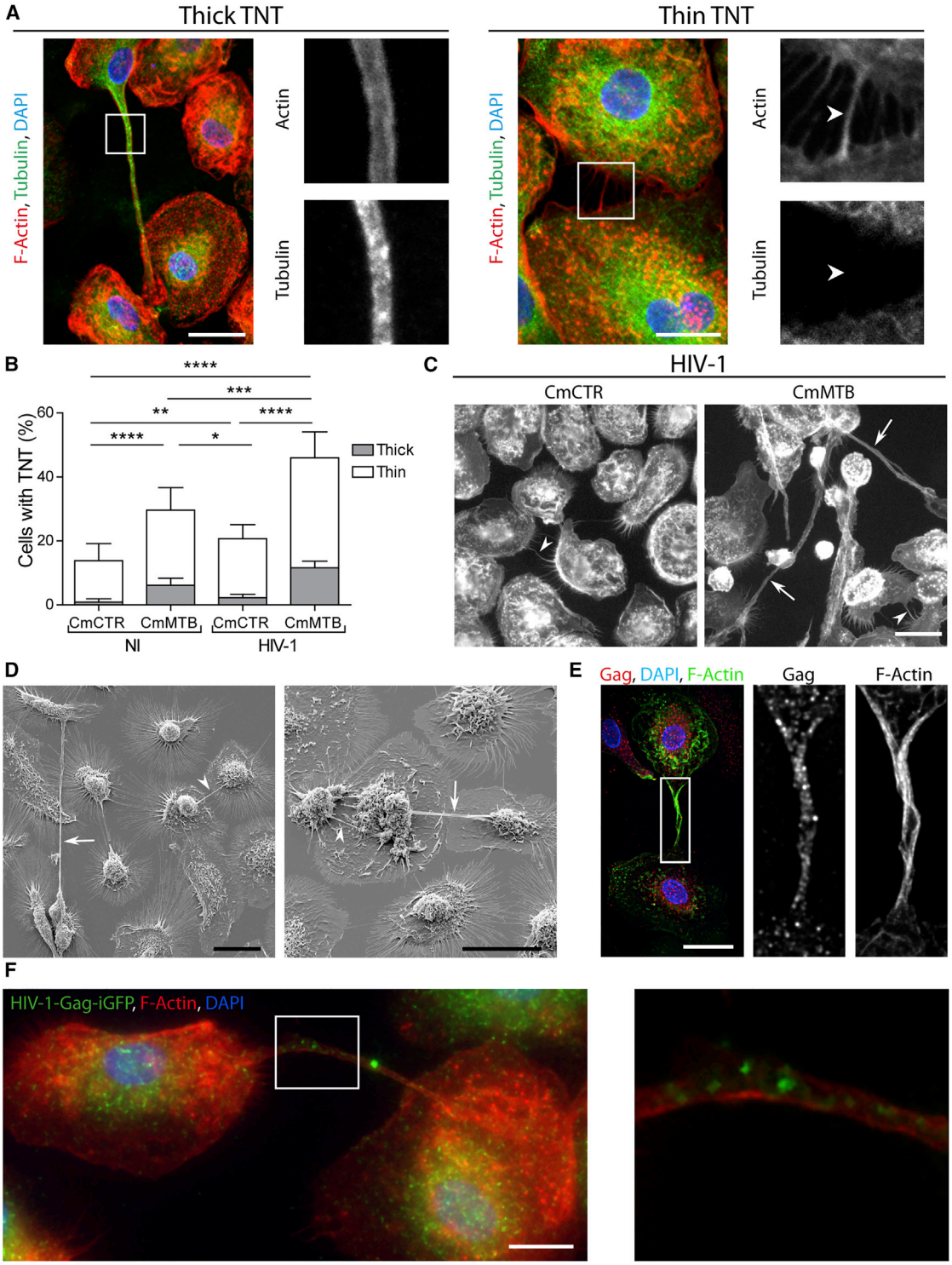

Figure 5. TB Enhances HIV-1-Induced TNT Formation

(A) Representative immunofluorescences image (IF) of macrophages interconnected through thick (left) and thin (right) TNTs. F-Actin (red), Tubulin (green), and DAPI (blue). Scale bar, 20 μm. The arrows point at the thin TNT without microtubules.

(B) Stacked bars showing the percentage of cells with thick (gray) and thin (white) TNTs of day 6 uninfected or HIV-1-infected macrophages treated with CmCTR or CmMTB. Data in histograms are represented as mean ± SD.

(C) Representative wide-field IF images showing F-actin staining in day 6 HIV-1-infected macrophages, treated with CmCTR or CmMTB. Arrows, thick TNTs; arrowheads, thin TNTs. Scale bar, 20 μm.

(legend continued on next page)

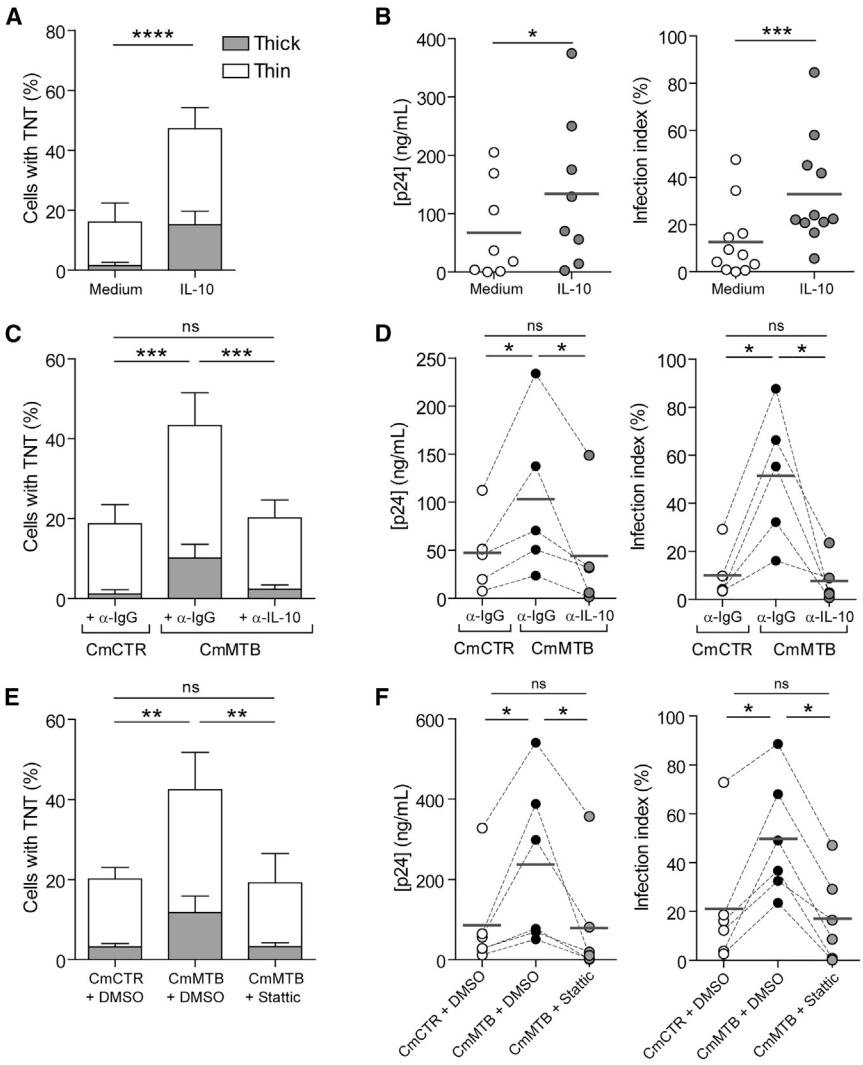

Figure 6. TB-Driven TNT Formation and Increased HIV-1 Infection Are Dependent on the IL-10/STAT3 Axis

(A) Stacked bars showing the percentage of cells with thick (gray) and thin (white) TNTs of day 6 HIV-1-infected macrophages untreated or treated with recombinant IL-10 (10 ng/mL).

(B) Vertical scatterplots showing p24 concentration (left) and infection index (right) of day 13 HIV-1-infected macrophages untreated or treated with recombinant IL-10 (10 ng/mL).

(C) Stacked bars showing the percentage of cells with thick (gray) and thin (white) TNTs of day 6 HIV-1-infected macrophages treated with IL-10-depleted (α-IL-10) CmMTB and mock depletion controls (α-IgG) of CmCTR and CmMTB.

(D) Vertical scatterplots showing p24 concentration (left) and infection index (right) of day 13 HIV-1-infected macrophages treated with IL-10-depleted (α-IL-10) CmMTB and mock depletion controls (α-IgG) of CmCTR and CmMTB.

(E) Stacked bars showing the percentage of cells with thick (gray) and thin (white) TNTs of day 6 HIV-1-infected macrophages treated with CmCTR, CmMTB, or CmMTB in the presence of the STAT3 activation inhibitor, Stattic (1 μM).

(F) Vertical scatterplots showing p24 release (left) and infection index (right) of day 13 HIV-1-infected macrophages treated with CmCTR, CmMTB, or CmMTB in the presence of the STAT3 activation inhibitor, Stattic (1 μM).

Statistical analyses: two-tailed, Wilcoxon matched-paired signed rank test (B and D, right, and F); paired t test (A–D, left, and E). *p ≤ 0.05; **p ≤ 0.005; ***p ≤ 0.0005; ns, not significant. See also Figures S2 and S6.

clinical challenge (Getahun et al., 2007), sCD163 and sMer may hold great promise as biomarkers in these populations.

Second, our study reveals that M(IL-10) macrophages are highly susceptible to HIV-1 infection. This is accompanied by enhanced MGC formation and protease-dependent migration capacity, which could play a role in HIV-1 dissemination (Vérollet et al., 2015b). All of these effects are fully dependent on the anti-inflammatory IL-10/STAT3 signaling pathway. Most of our work has been done with the ADA HIV-1 strain, which is a useful laboratory strain that can infect efficiently macrophages with low CD4 levels. However, these viruses are rather rare in the blood (Joseph and Swanstrom, 2018). As infected macrophages are found in the lungs (Bell and Noursadeghi, 2018; Cribbs et al., 2015), the characterization of the types of viruses mainly found in this co-infection sites (lung and pleural cavity) (Collins et al., 2002; Nakata et al., 1997; Singh et al., 1999) would be of great interest as we would have the opportunity to assess their effect in our model. Other reports also show that Mtb infection increases HIV-1 replication *in vitro* (Diedrich and Flynn, 2011; Goletti et al., 1998; Hoshino et al., 2002; Lederman et al., 1994; Zhang et al., 1995). However, unlike our study, they show that Mtb induces a pro-inflammatory environment resulting in the auto-activation of NF-κB, which ultimately binds the HIV-1 long terminal repeat (LTR) and initiates viral transcription in co-infected macrophages (Collins et al., 2002; Goletti et al., 1998,

(D) Scanning electron microscopy images showing TNTs of day 6 HIV-1-infected macrophages, treated with CmMTB. Arrows, thick TNTs; arrowheads, thin TNTs. Scale bar, 20 μm.

(E) Deconvolution microscopy images showing HIV-1 Gag intra-TNT distribution in day 6 HIV-1-infected macrophages, treated with CmMTB. HIV-1 Gag (red), F-actin (green), and DAPI (blue). Scale bar, 20 μm. Insets are 3× zooms.

(F) Immunofluorescence (IF) images showing viral particles in TNT of day 6 HIV-1-Gag-iGFP-infected macrophages previously treated with CmMTB. HIV-1-Gag-GFP (green), F-actin (red), and DAPI (blue). Scale bar, 10 μm. Inset is 4× zoom.

Statistical analyses: two-tailed paired t test (B). *p ≤ 0.05; **p ≤ 0.005; ***p ≤ 0.0005; ****p ≤ 0.0001; ns, not significant. See also Figure S5 and Video S3.

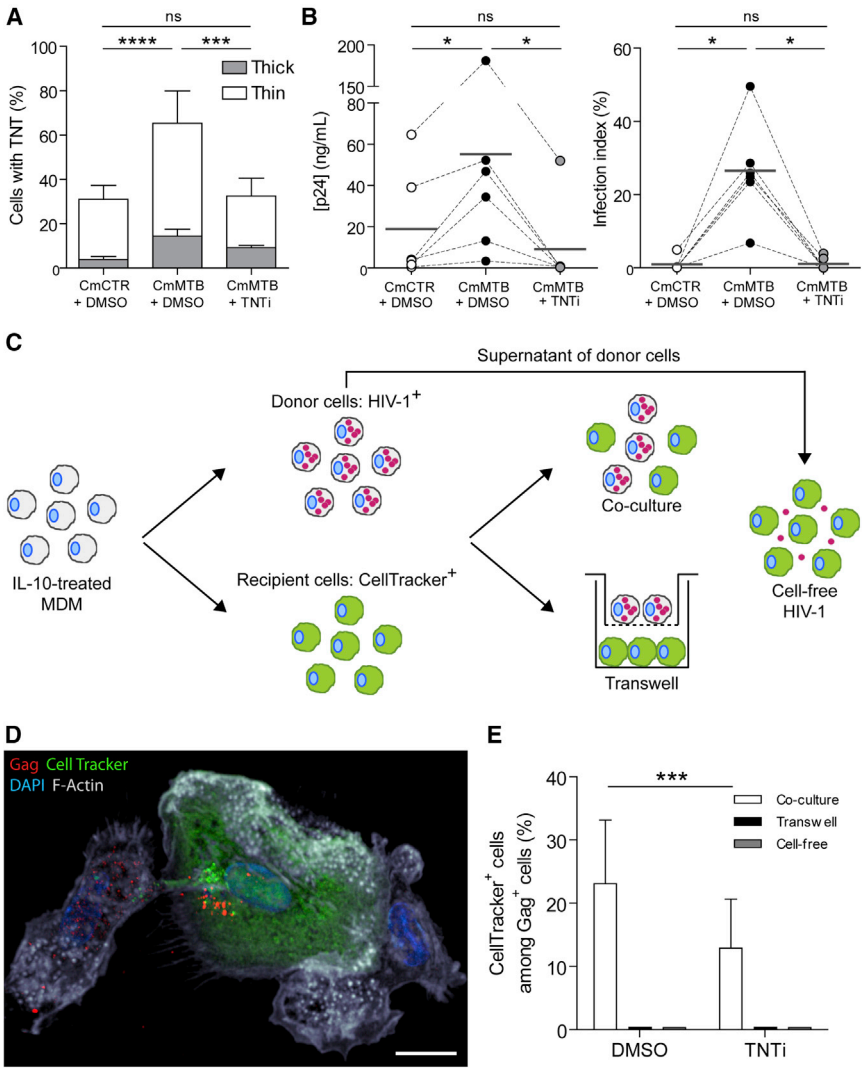

Figure 7. TB-Driven TNT Formation Is Necessary for Increased HIV-1 Infection

(A) Stacked bars showing the percentage of cells with thick (gray) and thin (white) TNTs of day 6 HIV-1-infected macrophages treated with CmCTR, CmMTB, or CmMTB in the presence of TNT inhibitor (TNTi, 20 μM).

(B) Vertical scatterplots showing p24 release (left) and infection index (right) of day 13 HIV-1-infected macrophages treated with CmCTR, CmMTB, or CmMTB in the presence of TNTi.

(C) Experimental setup used for the co-culture (also referred to as a transfer assay), Transwell, and cell-free HIV-1 experiments. IL-10-treated macrophages were either infected with HIV-1 NLAD8-VSVG pseudotyped strain at a MOI of 5 for 48 h (donor cells) or stained with CellTracker (acceptor cells). For the co-culture experiment, donor cells were mixed with acceptor cells at a 1:1 ratio. The Transwell assay was designed to separate donor and acceptor cells to investigate the contribution of cell contact to transfer of HIV-1. The experiment was performed as described in the co-culture assay, with the exception that acceptor cells were plated in the well, and then a Transwell filter was placed containing the donor cells. Finally, to assess the contribution of cell-free infection in the propagation of HIV-1, the supernatant of donor cells (containing the virions produced during 48 h of infection) was incubated with acceptor cells. To assess the contribution of TNTs in HIV-1 transfer, all three experiments were performed in the presence or not of TNTi (20 μM), and fixed after 24 h. The cells were stained for HIV-1 Gag protein, and the percentage of CellTracker$^+$ cells among Gag$^+$ cells was quantified.

(D) Deconvolution microscopy image showing HIV-1 Gag transfer into CellTracker$^+$ acceptor cell after 24-h co-culture. HIV-1 Gag (red), Cell Tracker (green), F-actin (gray), and DAPI (blue). Scale bar, 10 μm.

(E) Stacked bars showing the percentage of CellTracker$^+$ cells among Gag$^+$ cells after 24 h co-culture with or without TNTi (20 μM). Data in histograms are represented as mean ± SD. Each circle within the vertical scatterplots represents a single donor. Mean value is represented as a dark gray line. Statistical analyses: two-tailed, paired t test (A and E); Wilcoxon matched-paired signed rank test (B). *p ≤ 0.05; ***p ≤ 0.0005; ****p ≤ 0.0001; ns, not significant. See also Figure S7 and Videos S5 and S6.

2004; Hoshino et al., 2002; Lederman et al., 1994; Mancino et al., 1997; Nakata et al., 1997; Orenstein et al., 1997; Queval et al., 2016; Tanaka et al., 2005; Toossi, 2003; Zhang et al., 1995). Based on both these published observations and ours, we propose that TB exacerbates HIV-1 pathogenesis in a two-step manner: initially, by activating HIV-1 LTR transcription via short-lived pro-inflammatory signals in resident macrophages, and then by enhancing HIV-1 infection and spread in newly recruited monocytes predisposed toward the M(IL-10) phenotype, as a result of the anti-inflammatory signals induced by IL-10. This two-step model reconciles previous work done in co-infected cells and the results of our study, which is based on inherent susceptibility to HIV-1 infection observed in CD16$^+$ monocytes (Ellery et al., 2007) and macrophages derived from these cells (Ancuta et al., 2006). In light of recent evidence for macrophages as targets for HIV-1 pathogenesis (Honeycutt et al., 2016, 2017; Sattentau and Stevenson, 2016), together with the renewed appreciation of the importance of IL-10-driven anti-inflammatory program in macrophages (Ip et al., 2017), we believe that our *in vitro* model to generate M(IL-10) cells will help further characterize how TB influences viral infection of macrophages, and onward viral spread.

Third, based on our findings, we infer that TNT formation is likely a key cellular mechanism by which the IL-10/STAT3 signaling axis increases virus spread in human macrophages in a TB context. TNTs are transient membrane projections that facilitate intercellular communication to allow the transfer of endosomal cargo vesicles, calcium fluxes, and pathogens, such as bacteria, viruses, and prions (Davis and Sowinski, 2008; Dupont et al., 2018; Malik and Eugenin, 2016; McCoy-Simandle et al., 2016; Sherer and Mothes, 2008). In T cells, transmission of HIV-1 through TNTs is estimated to be approximately 100- to

1,000-fold more efficient than through classical cell-free viral infection (Sowinski et al., 2008). In macrophages, HIV-1 induces the formation of TNT via the protein Nef (Hashimoto et al., 2016; Xu et al., 2004). We confirmed that Nef is also involved in HIV-1-induced TNT formation in a TB-associated microenvironment (data not shown). Since the transmission of HIV-1 between macrophages via TNTs had not been formally demonstrated, we used here transwells to separate HIV-1-infected macrophages from uninfected macrophages, and we demonstrated that M(IL-10) macrophages are capable of transferring HIV-1 to non-infected macrophages through a cell-to-cell contact-dependent mechanism. While we cannot exclude the contribution of other cell-to-cell contact-dependent mechanisms of virus spread, such as virological synapse, cell fusion, phagocytosis, or efferocytosis (Baxter et al., 2014; Bracq et al., 2017; Jolly and Sattentau, 2004; Karaji and Sattentau, 2017), we clearly show that TNTs play a major role in this process. Pharmacological inhibition of TNT formation results in both reduced capacity of M(IL-10) macrophages to transfer viral particles and a substantial decrease of HIV-1 production. TNTs have been observed in several cell types and their formation is stimulated by different factors, including lipopolysaccharide (LPS) and interferon-γ (IFN-γ), pathogens, and oxidative stress, yet the signaling pathway(s) involved in TNT formation have not been identified (Ariazi et al., 2017; Dupont et al., 2018; Malik and Eugenin, 2016; Zhang, 2011). We reveal the IL-10/STAT3-axis as the main signaling pathway responsible for TNT formation between macrophages, providing an important contribution to this emerging field and paving the way for further elucidating the biology of TNTs. It would be interesting to find out whether TNTs could also form between M(IL-10) macrophages and other cell types, such as T or B cells, to transfer HIV-1 and/or viral material (Xu et al., 2009), which could participate in HIV-1 dissemination and pathogenesis within the co-infection context. Finally, whether TNTs are involved in MGC formation during HIV-1 infection of macrophages is suggested by a correlation between TNT formation and the number of MGCs that are formed ($r^2 = 0.7$ to 0.9). Another aspect that needs further improvement is the *in vivo* relevance of TNTs. Despite evidence for material transfer via TNT-like structures *in vivo* (Naphade et al., 2015; Rocca et al., 2017), the current lack of a specific TNT marker prevents the formal demonstration of existence of TNT *in vivo*. In pulmonary tissue lesions of co-infected NHPs, we observed TNT-like structures between $CD163^+$ macrophages, suggesting that cell-to-cell transfer of HIV-1 via TNTs could also occur *in vivo*. Indeed, M(IL-10) macrophages are in close proximity to each other, particularly in the lungs of co-infected NHPs, a parameter that is critical for TNT formation and viral transmission. Taking together our results, we propose that enhanced TNT formation induced by TB-associated microenvironment in M(IL-10) macrophages favors HIV-1 cell-to-cell transmission and, consequently, could play a key role in the high HIV-1 levels usually observed at anatomical sites of co-infection (Toossi, 2003).

In conclusion, this study highlights the importance of TB-associated microenvironment in shaping the response of macrophages to HIV-1 infection. Our results are highly relevant to the investigation of the role of macrophages in the pathogenesis of HIV-1/Mtb co-infection, cell signaling pathways involved in TNT formation, and the identification of potential biomarkers to monitor disease progression. Future research will reveal whether HIV-1 production and spread through TB-driven TNT formation occurs among M(IL-10) macrophages only, or also affects macrophage-to-T cell viral transmission (Groot et al., 2008), and whether TNT can be considered as a therapeutic target in co-infected patients.

STAR★METHODS

Detailed methods are provided in the online version of this paper and include the following:

- KEY RESOURCES TABLE
- CONTACT FOR REAGENT AND RESOURCE SHARING
- EXPERIMENTAL MODEL AND SUBJECT DETAILS
  - Human Subjects
  - NHPs
  - Bacteria
  - Viruses
  - Preparation of human monocytes and monocyte-derived macrophages
- METHODS DETAILS
  - Chemicals
  - Preparation of conditioned media and cytokine depletion
  - Conditioning of monocytes with the secretome of Mtb-infected macrophages or pleural effusions from TB patients
  - HIV-1 infection of cells
  - Blam-Vpr fusion assay
  - Flow cytometry
  - Immunofluorescence microscopy
  - HIV-1 and DiO transfer monitoring
  - Scanning electron microscopy
  - Immunoblot analyses
  - 3D migration assays
  - Protein quantifications in cell-free fluids by ELISA
  - Cytotoxicity assay
  - Phagocytosis assay
  - Histological analyses
- QUANTIFICATION AND STATISTICAL ANALYSIS

SUPPLEMENTAL INFORMATION

Supplemental Information can be found with this article online at https://doi.org/10.1016/j.celrep.2019.02.091.

ACKNOWLEDGMENTS

We greatly acknowledge F. Capilla and C. Salon (US006/CREFRE) and M. Ben Neji for histology analyses; M. Dubois, M. Cazabat, M. Requena, and J. Izopet (BiVic facility) and P. Constant, F. Levillain, F. Moreau, and C. Berrone (IPBS) (ASB3 and P3 multi-pathogens) for BSL3 facilities; I. Fourqueaux (CMEAB) for SEM imaging; T. Mangeat (LBCMCP) for deconvolution imaging; and A. Peixoto (IPBS) for imaging and flow cytometry analyses. The authors acknowledge the TRI-Genotoul and ANEXPLO facilities. We thank I. Gaillard and S. Caldirola (Immunology Division of the Hospital de Niños R. Gutiérrez, Buenos Aires) for their technical assistance. We greatly thank I. Staropoli and Z. Zhou (Pasteur Institute) for HIV-1 entry experiments, and C.A. Spinner

(IPBS), C. Gutierrez (IPBS), A. Moris (Cimi-Paris), and N. Iakobachvili (Maastricht University) for critical reading of the manuscript and helpful comments. This work was supported by Centre National de la Recherche Scientifique; Université Paul Sabatier; Agence Nationale de la Recherche (ANR 2010-01301, ANR14-CE11-0020-02, ANR16-CE13-0005-01, and ANR-11-EQUIPEX-0003); Agence Nationale de Recherche sur le Sida et les Hépatites Virales (ANRS2014-CI-2 and ANRS2014-049); the ECOS-Sud Program (A14S01); Fondation pour la Recherche Médicale (DEQ2016 0334894 and DEQ2016 0334902); Fondation Bettencourt Schueller, INSERM Plan Cancer; the Argentinean National Agency of Promotion of Science and Technology (PICT-2015-0055); and Alberto J. Roemmers Foundation (2016). We also thank the AIDS Research and Reference Reagent Program, Division of AIDS, NIAID. The NHP study was supported by NIH awards AI097059, AI110163, AI058609 and OD011104 to the Tulane National Primate Research Center and bridge fund by the Tulane Vice President for Research and awards by the Wetmore TB and Leprosy Foundation and the Louisiana Board of Regents. S.S. is supported by Sidaction and R.G. by ANRS.

AUTHOR CONTRIBUTIONS

Conceptualization & Methodology, S.S., L.B., M.d.C.S., O.N., I.M.-P., G.L.-V., and C.V.; Software, S.S. and R.P.; Investigation, S.S., L.B., M.D., K.P., C.L., D.K., C.C., A.B., R.G., R.P., and B.R.-M.; Resources, S.I., E.J.M., P.G.-M., S.P., and M.C.; Writing, S.S., O.N., I.M.-P., G.L.-V., and C.V.; Visualization, S.S.; Supervision, O.N., I.M.-P., G.L.-V., and C.V. Corresponding authors G.L.-V. and C.V. are responsible for ownership and responsibility that are inherent to aspects of tuberculosis (G.L.-V.) and HIV-1 (C.V.).

DECLARATION OF INTERESTS

The authors declare no competing interests.

Received: August 23, 2018
Revised: December 8, 2018
Accepted: February 21, 2019
Published: March 26, 2019

REFERENCES

Ancuta, P., Wang, J., and Gabuzda, D. (2006). $CD16^+$ monocytes produce IL-6, CCL2, and matrix metalloproteinase-9 upon interaction with CX3CL1-expressing endothelial cells. J. Leukoc. Biol. *80*, 1156–1164.

Ariazi, J., Benowitz, A., De Biasi, V., Den Boer, M.L., Cherqui, S., Cui, H., Douillet, N., Eugenin, E.A., Favre, D., Goodman, S., et al. (2017). Tunneling nanotubes and gap junctions-their role in long-range intercellular communication during development, health, and disease conditions. Front. Mol. Neurosci. *10*, 333.

Avalos, C.R., Price, S.L., Forsyth, E.R., Pin, J.N., Shirk, E.N., Bullock, B.T., Queen, S.E., Li, M., Gellerup, D., O'Connor, S.L., et al. (2016). Quantitation of productively infected monocytes and macrophages of simian immunodeficiency virus-infected macaques. J. Virol. *90*, 5643–5656.

Balboa, L., Romero, M.M., Basile, J.I., Sabio y García, C.A., Schierloh, P., Yokobori, N., Geffner, L., Musella, R.M., Castagnino, J., Abbate, E., et al. (2011). Paradoxical role of $CD16^+CCR2^+CCR5^+$ monocytes in tuberculosis: efficient APC in pleural effusion but also mark disease severity in blood. J. Leukoc. Biol. *90*, 69–75.

Baxter, A.E., Russell, R.A., Duncan, C.J., Moore, M.D., Willberg, C.B., Pablos, J.L., Finzi, A., Kaufmann, D.E., Ochsenbauer, C., Kappes, J.C., et al. (2014). Macrophage infection via selective capture of HIV-1-infected CD4+ T cells. Cell Host Microbe *16*, 711–721.

Bell, L.C.K., and Noursadeghi, M. (2018). Pathogenesis of HIV-1 and *Mycobacterium tuberculosis* co-infection. Nat. Rev. Microbiol. *16*, 80–90.

Bracq, L., Xie, M., Lambelé, M., Vu, L.T., Matz, J., Schmitt, A., Delon, J., Zhou, P., Randriamampita, C., Bouchet, J., and Benichou, S. (2017). T cell-macrophage fusion triggers multinucleated giant cell formation for HIV-1 spreading. J. Virol. Published online October 4, 2017. https://doi.org/10.1128/JVI.01237-17.

Burdo, T.H., Soulas, C., Orzechowski, K., Button, J., Krishnan, A., Sugimoto, C., Alvarez, X., Kuroda, M.J., and Williams, K.C. (2010). Increased monocyte turnover from bone marrow correlates with severity of SIV encephalitis and CD163 levels in plasma. PLoS Pathog. *6*, e1000842.

Burdo, T.H., Lentz, M.R., Autissier, P., Krishnan, A., Halpern, E., Letendre, S., Rosenberg, E.S., Ellis, R.J., and Williams, K.C. (2011). Soluble CD163 made by monocyte/macrophages is a novel marker of HIV activity in early and chronic infection prior to and after anti-retroviral therapy. J. Infect. Dis. *204*, 154–163.

Cai, Y., Sugimoto, C., Liu, D.X., Midkiff, C.C., Alvarez, X., Lackner, A.A., Kim, W.K., Didier, E.S., and Kuroda, M.J. (2015). Increased monocyte turnover is associated with interstitial macrophage accumulation and pulmonary tissue damage in SIV-infected rhesus macaques. J. Leukoc. Biol. *97*, 1147–1153.

Cassol, E., Cassetta, L., Rizzi, C., Alfano, M., and Poli, G. (2009). M1 and M2a polarization of human monocyte-derived macrophages inhibits HIV-1 replication by distinct mechanisms. J. Immunol. *182*, 6237–6246.

Cavrois, M., De Noronha, C., and Greene, W.C. (2002). A sensitive and specific enzyme-based assay detecting HIV-1 virion fusion in primary T lymphocytes. Nat. Biotechnol. *20*, 1151–1154.

Charles, T.P., and Shellito, J.E. (2016). Human immunodeficiency virus infection and host defense in the lungs. Semin. Respir. Crit. Care Med. *37*, 147–156.

Collins, K.R., Quiñones-Mateu, M.E., Wu, M., Luzze, H., Johnson, J.L., Hirsch, C., Toossi, Z., and Arts, E.J. (2002). Human immunodeficiency virus type 1 (HIV-1) quasispecies at the sites of *Mycobacterium tuberculosis* infection contribute to systemic HIV-1 heterogeneity. J. Virol. *76*, 1697–1706.

Cribbs, S.K., Lennox, J., Caliendo, A.M., Brown, L.A., and Guidot, D.M. (2015). Healthy HIV-1-infected individuals on highly active antiretroviral therapy harbor HIV-1 in their alveolar macrophages. AIDS Res. Hum. Retroviruses *31*, 64–70.

Davis, D.M., and Sowinski, S. (2008). Membrane nanotubes: dynamic long-distance connections between animal cells. Nat. Rev. Mol. Cell Biol. *9*, 431–436.

Diedrich, C.R., and Flynn, J.L. (2011). HIV-1/*Mycobacterium tuberculosis* coinfection immunology: how does HIV-1 exacerbate tuberculosis? Infect. Immun. *79*, 1407–1417.

Diedrich, C.R., O'Hern, J., and Wilkinson, R.J. (2016). HIV-1 and the *Mycobacterium tuberculosis* granuloma: a systematic review and meta-analysis. Tuberculosis (Edinb.) *98*, 62–76.

Dupont, M., Souriant, S., Lugo-Villarino, G., Maridonneau-Parini, I., and Vérollet, C. (2018). Tunneling nanotubes: intimate communication between myeloid cells. Front. Immunol. *9*, 43.

Ellery, P.J., Tippett, E., Chiu, Y.L., Paukovics, G., Cameron, P.U., Solomon, A., Lewin, S.R., Gorry, P.R., Jaworowski, A., Greene, W.C., et al. (2007). The $CD16^+$ monocyte subset is more permissive to infection and preferentially harbors HIV-1 in vivo. J. Immunol. *178*, 6581–6589.

Esmail, H., Riou, C., du Bruyn, E., Lai, R.P., Harley, Y.X.R., Meintjes, G., Wilkinson, K.A., and Wilkinson, R.J. (2018). The immune response to *Mycobacterium tuberculosis* in HIV-1-coinfected persons. Annu. Rev. Immunol. *36*, 603–638.

Espert, L., Beaumelle, B., and Vergne, I. (2015). Autophagy in *Mycobacterium tuberculosis* and HIV infections. Front. Cell. Infect. Microbiol. *5*, 49.

Eugenin, E.A., Gaskill, P.J., and Berman, J.W. (2009). Tunneling nanotubes (TNT) are induced by HIV-infection of macrophages: a potential mechanism for intercellular HIV trafficking. Cell. Immunol. *254*, 142–148.

Fabriek, B.O., Dijkstra, C.D., and van den Berg, T.K. (2005). The macrophage scavenger receptor CD163. Immunobiology *210*, 153–160.

Foreman, T.W., Mehra, S., LoBato, D.N., Malek, A., Alvarez, X., Golden, N.A., Bucşan, A.N., Didier, P.J., Doyle-Meyers, L.A., Russell-Lodrigue, K.E., et al. (2016). $CD4^+$ T-cell-independent mechanisms suppress reactivation of latent tuberculosis in a macaque model of HIV coinfection. Proc. Natl. Acad. Sci. USA *113*, E5636–E5644.

Garcia-Perez, J., Staropoli, I., Azoulay, S., Heinrich, J.T., Cascajero, A., Colin, P., Lortat-Jacob, H., Arenzana-Seisdedos, F., Alcami, J., Kellenberger, E., and

Lagane, B. (2015). A single-residue change in the HIV-1 V3 loop associated with maraviroc resistance impairs CCR5 binding affinity while increasing replicative capacity. Retrovirology *12*, 50.

Gaudin, R., Berre, S., Cunha de Alencar, B., Decalf, J., Schindler, M., Gobert, F.X., Jouve, M., and Benaroch, P. (2013). Dynamics of HIV-containing compartments in macrophages reveal sequestration of virions and transient surface connections. PLoS ONE *8*, e69450.

Genoula, M., Marín Franco, J.L., Dupont, M., Kviatcovsky, D., Milillo, A., Schierloh, P., Moraña, E.J., Poggi, S., Palmero, D., Mata-Espinosa, D., et al. (2018). Formation of foamy macrophages by tuberculous pleural effusions is triggered by the interleukin-10/signal transducer and activator of transcription 3 axis through ACAT upregulation. Front. Immunol. *9*, 459.

Getahun, H., Harrington, M., O'Brien, R., and Nunn, P. (2007). Diagnosis of smear-negative pulmonary tuberculosis in people with HIV infection or AIDS in resource-constrained settings: informing urgent policy changes. Lancet *369*, 2042–2049.

Goletti, D., Weissman, D., Jackson, R.W., Collins, F., Kinter, A., and Fauci, A.S. (1998). The in vitro induction of human immunodeficiency virus (HIV) replication in purified protein derivative-positive HIV-infected persons by recall antigen response to *Mycobacterium tuberculosis* is the result of a balance of the effects of endogenous interleukin-2 and proinflammatory and antiinflammatory cytokines. J. Infect. Dis. *177*, 1332–1338.

Goletti, D., Carrara, S., Vincenti, D., Giacomini, E., Fattorini, L., Garbuglia, A.R., Capobianchi, M.R., Alonzi, T., Fimia, G.M., Federico, M., et al. (2004). Inhibition of HIV-1 replication in monocyte-derived macrophages by *Mycobacterium tuberculosis*. J. Infect. Dis. *189*, 624–633.

Gordon, S., Plüddemann, A., and Martinez Estrada, F. (2014). Macrophage heterogeneity in tissues: phenotypic diversity and functions. Immunol. Rev. *262*, 36–55.

Groot, F., Welsch, S., and Sattentau, Q.J. (2008). Efficient HIV-1 transmission from macrophages to T cells across transient virological synapses. Blood *111*, 4660–4663.

Hase, K., Kimura, S., Takatsu, H., Ohmae, M., Kawano, S., Kitamura, H., Ito, M., Watarai, H., Hazelett, C.C., Yeaman, C., and Ohno, H. (2009). M-Sec promotes membrane nanotube formation by interacting with Ral and the exocyst complex. Nat. Cell Biol. *11*, 1427–1432.

Hashimoto, M., Bhuyan, F., Hiyoshi, M., Noyori, O., Nasser, H., Miyazaki, M., Saito, T., Kondoh, Y., Osada, H., Kimura, S., et al. (2016). Potential role of the formation of tunneling nanotubes in HIV-1 spread in macrophages. J. Immunol. *196*, 1832–1841.

Honeycutt, J.B., Wahl, A., Baker, C., Spagnuolo, R.A., Foster, J., Zakharova, O., Wietgrefe, S., Caro-Vegas, C., Madden, V., Sharpe, G., et al. (2016). Macrophages sustain HIV replication in vivo independently of T cells. J. Clin. Invest. *126*, 1353–1366.

Honeycutt, J.B., Thayer, W.O., Baker, C.E., Ribeiro, R.M., Lada, S.M., Cao, Y., Cleary, R.A., Hudgens, M.G., Richman, D.D., and Garcia, J.V. (2017). HIV persistence in tissue macrophages of humanized myeloid-only mice during antiretroviral therapy. Nat. Med. *23*, 638–643.

Hoshino, Y., Nakata, K., Hoshino, S., Honda, Y., Tse, D.B., Shioda, T., Rom, W.N., and Weiden, M. (2002). Maximal HIV-1 replication in alveolar macrophages during tuberculosis requires both lymphocyte contact and cytokines. J. Exp. Med. *195*, 495–505.

Ip, W.K.E., Hoshi, N., Shouval, D.S., Snapper, S., and Medzhitov, R. (2017). Anti-inflammatory effect of IL-10 mediated by metabolic reprogramming of macrophages. Science *356*, 513–519.

Jolly, C., and Sattentau, Q.J. (2004). Retroviral spread by induction of virological synapses. Traffic *5*, 643–650.

Joseph, S.B., and Swanstrom, R. (2018). The evolution of HIV-1 entry phenotypes as a guide to changing target cells. J. Leukoc. Biol. *103*, 421–431.

Karaji, N., and Sattentau, Q.J. (2017). Efferocytosis of pathogen-infected cells. Front. Immunol. *8*, 1863.

Kaushal, D., Mehra, S., Didier, P.J., and Lackner, A.A. (2012). The non-human primate model of tuberculosis. J. Med. Primatol. *41*, 191–201.

Khan, N., and Divangahi, M. (2018). *Mycobacterium tuberculosis* and HIV co-infection brings fire and fury to macrophages. J. Infect. Dis. *217*, 1851–1853.

Knudsen, T.B., Gustafson, P., Kronborg, G., Kristiansen, T.B., Moestrup, S.K., Nielsen, J.O., Gomes, V., Aaby, P., Lisse, I., Moller, H.J., et al. (2005). Predictive value of soluble haemoglobin scavenger receptor CD163 serum levels for survival in verified tuberculosis patients. Clin. Microbiol. Infect. *11*, 730–735.

Kuroda, M.J., Sugimoto, C., Cai, Y., Merino, K.M., Mehra, S., Araínga, M., Roy, C.J., Midkiff, C.C., Alvarez, X., Didier, E.S., and Kaushal, D. (2018). High turnover of tissue macrophages contributes to tuberculosis reactivation in simian immunodeficiency virus-infected rhesus macaques. J. Infect. Dis. *217*, 1865–1874.

Laguette, N., Sobhian, B., Casartelli, N., Ringeard, M., Chable-Bessia, C., Ségéral, E., Yatim, A., Emiliani, S., Schwartz, O., and Benkirane, M. (2011). SAMHD1 is the dendritic- and myeloid-cell-specific HIV-1 restriction factor counteracted by Vpx. Nature *474*, 654–657.

Lastrucci, C., Bénard, A., Balboa, L., Pingris, K., Souriant, S., Poincloux, R., Al Saati, T., Rasolofo, V., González-Montaner, P., Inwentarz, S., et al. (2015). Tuberculosis is associated with expansion of a motile, permissive and immunomodulatory $CD16^+$ monocyte population via the IL-10/STAT3 axis. Cell Res. *25*, 1333–1351.

Lawn, S.D., Pisell, T.L., Hirsch, C.S., Wu, M., Butera, S.T., and Toossi, Z. (2001). Anatomically compartmentalized human immunodeficiency virus replication in $HLA\text{-}DR^+$ cells and $CD14^+$ macrophages at the site of pleural tuberculosis coinfection. J. Infect. Dis. *184*, 1127–1133.

Le Cabec, V., and Maridonneau-Parini, I. (1994). Annexin 3 is associated with cytoplasmic granules in neutrophils and monocytes and translocates to the plasma membrane in activated cells. Biochem. J. *303*, 481–487.

Le Cabec, V., Cols, C., and Maridonneau-Parini, I. (2000). Nonopsonic phagocytosis of zymosan and *Mycobacterium kansasii* by CR3 (CD11b/CD18) involves distinct molecular determinants and is or is not coupled with NADPH oxidase activation. Infect. Immun. *68*, 4736–4745.

Lederman, M.M., Georges, D.L., Kusner, D.J., Mudido, P., Giam, C.Z., and Toossi, Z. (1994). *Mycobacterium tuberculosis* and its purified protein derivative activate expression of the human immunodeficiency virus. J. Acquir. Immune Defic. Syndr. *7*, 727–733.

Light, R.W. (2010). Update on tuberculous pleural effusion. Respirology *15*, 451–458.

Lugo-Villarino, G., Vérollet, C., Maridonneau-Parini, I., and Neyrolles, O. (2011). Macrophage polarization: convergence point targeted by *Mycobacterium tuberculosis* and HIV. Front. Immunol. *2*, 43.

Malik, S., and Eugenin, E.A. (2016). Mechanisms of HIV neuropathogenesis: role of cellular communication systems. Curr. HIV Res. *14*, 400–411.

Mancino, G., Placido, R., Bach, S., Mariani, F., Montesano, C., Ercoli, L., Zembala, M., and Colizzi, V. (1997). Infection of human monocytes with *Mycobacterium tuberculosis* enhances human immunodeficiency virus type 1 replication and transmission to T cells. J. Infect. Dis. *175*, 1531–1535.

Maridonneau-Parini, I. (2014). Control of macrophage 3D migration: a therapeutic challenge to limit tissue infiltration. Immunol. Rev. *262*, 216–231.

McCoy-Simandle, K., Hanna, S.J., and Cox, D. (2016). Exosomes and nanotubes: control of immune cell communication. Int. J. Biochem. Cell Biol. *71*, 44–54.

Mehra, S., Golden, N.A., Dutta, N.K., Midkiff, C.C., Alvarez, X., Doyle, L.A., Asher, M., Russell-Lodrigue, K., Monjure, C., Roy, C.J., et al. (2011). Reactivation of latent tuberculosis in rhesus macaques by coinfection with simian immunodeficiency virus. J. Med. Primatol. *40*, 233–243.

Murray, P.J., Allen, J.E., Biswas, S.K., Fisher, E.A., Gilroy, D.W., Goerdt, S., Gordon, S., Hamilton, J.A., Ivashkiv, L.B., Lawrence, T., et al. (2014). Macrophage activation and polarization: nomenclature and experimental guidelines. Immunity *41*, 14–20.

Nakata, K., Rom, W.N., Honda, Y., Condos, R., Kanegasaki, S., Cao, Y., and Weiden, M. (1997). *Mycobacterium tuberculosis* enhances human immunodeficiency virus-1 replication in the lung. Am. J. Respir. Crit. Care Med. *155*, 996–1003.

Naphade, S., Sharma, J., Gaide Chevronnay, H.P., Shook, M.A., Yeagy, B.A., Rocca, C.J., Ur, S.N., Lau, A.J., Courtoy, P.J., and Cherqui, S. (2015). Brief reports: lysosomal cross-correction by hematopoietic stem cell-derived macrophages via tunneling nanotubes. Stem Cells *33*, 301–309.

O'Garra, A., Redford, P.S., McNab, F.W., Bloom, C.I., Wilkinson, R.J., and Berry, M.P. (2013). The immune response in tuberculosis. Annu. Rev. Immunol. *31*, 475–527.

Okafo, G., Prevedel, L., and Eugenin, E. (2017). Tunneling nanotubes (TNT) mediate long-range gap junctional communication: implications for HIV cell to cell spread. Sci. Rep. *7*, 16660.

Onfelt, B., Nedvetzki, S., Benninger, R.K., Purbhoo, M.A., Sowinski, S., Hume, A.N., Seabra, M.C., Neil, M.A., French, P.M., and Davis, D.M. (2006). Structurally distinct membrane nanotubes between human macrophages support long-distance vesicular traffic or surfing of bacteria. J. Immunol. *177*, 8476–8483.

Orenstein, J.M. (2000). In vivo cytolysis and fusion of human immunodeficiency virus type 1-infected lymphocytes in lymphoid tissue. J. Infect. Dis. *182*, 338–342.

Orenstein, J.M. (2001). The macrophage in HIV infection. Immunobiology *204*, 598–602.

Orenstein, J.M., Fox, C., and Wahl, S.M. (1997). Macrophages as a source of HIV during opportunistic infections. Science *276*, 1857–1861.

Queval, C.J., Song, O.R., Deboosère, N., Delorme, V., Debrie, A.S., Iantomasi, R., Veyron-Churlet, R., Jouny, S., Redhage, K., Deloison, G., et al. (2016). STAT3 represses nitric oxide synthesis in human macrophages upon *Mycobacterium tuberculosis* infection. Sci. Rep. *6*, 29297.

Raynaud-Messina, B., Bracq, L., Dupont, M., Souriant, S., Usmani, S.M., Proag, A., Pingris, K., Soldan, V., Thibault, C., Capilla, F., et al. (2018). Bone degradation machinery of osteoclasts: an HIV-1 target that contributes to bone loss. Proc. Natl. Acad. Sci. USA *115*, E2556–E2565.

Rocca, C.J., Goodman, S.M., Dulin, J.N., Haquang, J.H., Gertsman, I., Blondelle, J., Smith, J.L.M., Heyser, C.J., and Cherqui, S. (2017). Transplantation of wild-type mouse hematopoietic stem and progenitor cells ameliorates deficits in a mouse model of Friedreich's ataxia. Sci. Transl. Med. *9*, eaaj2347.

Russell, D.G., Barry, C.E., 3rd, and Flynn, J.L. (2010). Tuberculosis: what we don't know can, and does, hurt us. Science *328*, 852–856.

Sather, S., Kenyon, K.D., Lefkowitz, J.B., Liang, X., Varnum, B.C., Henson, P.M., and Graham, D.K. (2007). A soluble form of the Mer receptor tyrosine kinase inhibits macrophage clearance of apoptotic cells and platelet aggregation. Blood *109*, 1026–1033.

Sattentau, Q.J., and Stevenson, M. (2016). Macrophages and HIV-1: an unhealthy constellation. Cell Host Microbe *19*, 304–310.

Schierloh, P., Yokobori, N., Alemán, M., Landoni, V., Geffner, L., Musella, R.M., Castagnino, J., Baldini, M., Abbate, E., de la Barrera, S.S., and Sasiain, M.C. (2007). *Mycobacterium tuberculosis*-induced gamma interferon production by natural killer cells requires cross talk with antigen-presenting cells involving Toll-like receptors 2 and 4 and the mannose receptor in tuberculous pleurisy. Infect. Immun. *75*, 5325–5337.

Sherer, N.M., and Mothes, W. (2008). Cytonemes and tunneling nanotubules in cell-cell communication and viral pathogenesis. Trends Cell Biol. *18*, 414–420.

Singh, A., Besson, G., Mobasher, A., and Collman, R.G. (1999). Patterns of chemokine receptor fusion cofactor utilization by human immunodeficiency virus type 1 variants from the lungs and blood. J. Virol. *73*, 6680–6690.

Sowinski, S., Jolly, C., Berninghausen, O., Purbhoo, M.A., Chauveau, A., Köhler, K., Oddos, S., Eissmann, P., Brodsky, F.M., Hopkins, C., et al. (2008). Membrane nanotubes physically connect T cells over long distances presenting a novel route for HIV-1 transmission. Nat. Cell Biol. *10*, 211–219.

Tanaka, N., Hoshino, Y., Gold, J., Hoshino, S., Martiniuk, F., Kurata, T., Pine, R., Levy, D., Rom, W.N., and Weiden, M. (2005). Interleukin-10 induces inhibitory C/EBPbeta through STAT-3 and represses HIV-1 transcription in macrophages. Am. J. Respir. Cell Mol. Biol. *33*, 406–411.

Tomlinson, G.S., Bell, L.C., Walker, N.F., Tsang, J., Brown, J.S., Breen, R., Lipman, M., Katz, D.R., Miller, R.F., Chain, B.M., et al. (2013). HIV-1 infection of macrophages dysregulates innate immune responses to *Mycobacterium tuberculosis* by inhibition of interleukin-10. J. Infect. Dis. *209*, 1055–1065.

Toossi, Z. (2003). Virological and immunological impact of tuberculosis on human immunodeficiency virus type 1 disease. J. Infect. Dis. *188*, 1146–1155.

Toossi, Z., Nicolacakis, K., Xia, L., Ferrari, N.A., and Rich, E.A. (1997). Activation of latent HIV-1 by *Mycobacterium tuberculosis* and its purified protein derivative in alveolar macrophages from HIV-infected individuals in vitro. J. Acquir. Immune Defic. Syndr. Hum. Retrovirol. *15*, 325–331.

Vérollet, C., Zhang, Y.M., Le Cabec, V., Mazzolini, J., Charrière, G., Labrousse, A., Bouchet, J., Medina, I., Biessen, E., Niedergang, F., et al. (2010). HIV-1 Nef triggers macrophage fusion in a p61Hck- and protease-dependent manner. J. Immunol. *184*, 7030–7039.

Vérollet, C., Souriant, S., Bonnaud, E., Jolicoeur, P., Raynaud-Messina, B., Kinnaer, C., Fourquaux, I., Imle, A., Benichou, S., Fackler, O.T., et al. (2015a). HIV-1 reprograms the migration of macrophages. Blood *125*, 1611–1622.

Vérollet, C., Souriant, S., Raynaud-Messina, B., and Maridonneau-Parini, I. (2015b). [HIV-1 drives the migration of macrophages]. Med. Sci. (Paris) *31*, 730–733.

Vorster, M.J., Allwood, B.W., Diacon, A.H., and Koegelenberg, C.F. (2015). Tuberculous pleural effusions: advances and controversies. J. Thorac. Dis. *7*, 981–991.

Xu, Y., Kulkosky, J., Acheampong, E., Nunnari, G., Sullivan, J., and Pomerantz, R.J. (2004). HIV-1-mediated apoptosis of neuronal cells: proximal molecular mechanisms of HIV-1-induced encephalopathy. Proc. Natl. Acad. Sci. USA *101*, 7070–7075.

Xu, W., Santini, P.A., Sullivan, J.S., He, B., Shan, M., Ball, S.C., Dyer, W.B., Ketas, T.J., Chadburn, A., Cohen-Gould, L., et al. (2009). HIV-1 evades virus-specific IgG2 and IgA responses by targeting systemic and intestinal B cells via long-range intercellular conduits. Nat. Immunol. *10*, 1008–1017.

Zhang, Y. (2011). Tunneling-nanotube: a new way of cell-cell communication. Commun. Integr. Biol. *4*, 324–325.

Zhang, Y., Nakata, K., Weiden, M., and Rom, W.N. (1995). *Mycobacterium tuberculosis* enhances human immunodeficiency virus-1 replication by transcriptional activation at the long terminal repeat. J. Clin. Invest. *95*, 2324–2331.

Ziegler-Heitbrock, L. (2007). The $CD14^+$ $CD16^+$ blood monocytes: their role in infection and inflammation. J. Leukoc. Biol. *81*, 584–592.

STAR★METHODS

KEY RESOURCES TABLE

REAGENT or RESOURCE	SOURCE	IDENTIFIER
Antibodies		
Anti-human CD14	Biolegend	Clone M5E2; RRID:AB_893250
Anti-human CD16	Biolegend	Clone 3G8; RRID:AB_314206
Anti-human CD163	Biolegend	Clone GHI/61; RRID:AB_1134002
Anti-human CD184 (CXCR4)	Biolegend	Clone 12G5; RRID:AB_10642818
Anti-human CD195 (CCR5)	Biolegend	Clone J418F1; RRID:AB_2564073
Anti-human CD274 (B7-H1, PD-L1)	Biolegend	Clone 29E.2A3; RRID:AB_940366
Anti-human CD4	Biolegend	Clone RPA-T4; RRID:AB_314082
Anti-human CD64	Biolegend	Clone 10.1; RRID:AB_2734691
Anti-human CD86	Biolegend	Clone IT2.2; RRID:AB_2074981
Anti-human HLA-DR	Biolegend	Clone L243; RRID:AB_2572101
Anti-human MerTK	Biolegend	Clone 590H11G1E3; RRID: AB_2687286
Anti-human STAT3	Cell Signaling Technology	Clone D1A5; https://media.cellsignal.com/pdf/8768.pdf
Anti-human phosphoTyr705-STAT3	Cell Signaling Technology	Clone D3A7; https://media.cellsignal.com/pdf/9145.pdf
Anti-human SAMHD1	Gift from Dr. O Schwartz Institut Pasteur, Paris, France	Laguette et al., 2011
Anti-human phosphoThr592-SAMHD1	ProSci	Cat# 8005; RRID:AB_2316381
Anti-human IFITM1/2/3	Santa Cruz Biotechnology	Clone FL-125; http://datasheets.scbt.com/sc-66827.pdf
Anti-human C/EBP-β	Santa Cruz Biotechnology	Clone H-7; https://datasheets.scbt.com/sc-7962.pdf
Anti-human CUGBP1	Santa Cruz Biotechnology	Clone 3B1; RRID:AB_627319
Anti-human Actin	Sigma-Aldrich	Clone 20-33; RRID:AB_476738
Anti-human LC3	Sigma-Aldrich	Cat# L8918; RRID:AB_1079382
Anti-human Gag-RD1	Beckman Coulter	Clone KC57; https://www.bc-cytometry.com/PDF/DataSheet/6604665&6604667%20D.S.pdf
Anti-human CD163	Leica/Novocastra	Clone 10D6; RRID:AB_2756375
Anti-human alpha-tubulin	Sigma-Aldrich	clone B-5-1-2; RRID:AB_477582
LEAF purified anti-human IL-10	Biolegend	Clone JES3-19F1; RRID:AB_315460
LEAF purified rat anti-human IgG2a	Biolegend	Clone RTK2758; RRID:AB_326523
Goat anti-rabbit IgG, AlexaFluor 555	Thermo Fisher Scientific	Cat# A-21430; RRID:AB_2535851
Goat anti-mouse IgG, AlexaFluor 488	Thermo Fisher Scientific	Cat# A-10684; RRID:AB_2534064
Goat anti-Mouse IgG, AlexaFluor 555	Cell Signaling Technology	Cat# 4409; RRID:AB_1904022
Goat anti-rabbit IgG, HRP	Thermo Fisher Scientific	Cat# 32460; RRID:AB_1185567
Goat anti-mouse IgG, HRP	Thermo Fisher Scientific	Cat# 31430; RRID:AB_228307
Bacterial and Virus Strains		
M. tuberculosis H37Rv	N/A	N/A
HIV-1 ADA strain	Gift from Dr. S Benichou Institut Cochin, Paris, France	Vérollet et al., 2015a
HIV-1 ADA Gag-iGFP strain	Gift from Dr P. Benaroch Institut Pasteur, Paris, France	Gaudin et al., 2013
HIV-1 NLAD8-VSVG	Gift from Dr. S Benichou Institut Cochin, Paris, France	Bracq et al., 2017
HIV-1 ADA (BlaM-Vpr)	N/A	N/A

(*Continued on next page*)

Continued

REAGENT or RESOURCE	SOURCE	IDENTIFIER
Biological Samples		
Buffy Coat	Etablissement Français du Sang, Toulouse, France	N/A
Patients-derived pleural effusions	División de Tisioneumonología at the Instituto de Tisioneumonología Vaccarezza-University of Buenos Aires, Argentina	N/A
TB patients-derived peripheral blood	División de Tisioneumonología at the Instituto de Tisioneumonología Vaccarezza-University of Buenos Aires, Argentina	N/A
HIV/TB patients-derived peripheral blood	Division de SIDA at the Hospital F.J Muñiz, Buenos Aires, Argentina	N/A
Healthy subjects-derived peripheral blood	Blood Transfusion Service, *Hospital Fernandez*, Buenos Aires, Argentina	N/A
Histological slides of lung biopsies from rhesus macaques	Tulane National Primate Research Center	N/A
Chemicals, Peptides, and Recombinant Proteins		
Human M-CSF	Peprotech	Cat# 300-25
Stattic	Sigma-Aldrich	Cat# S7947
TNTi	Pharmeks	N/A
Cytochalasin D	Sigma-Aldrich	Cat# 22144-77-0
Maraviroc	Sigma-Aldrich	Cat# 376348-65-1
Bafilomycin A1	Sigma-Aldrich	Cat# 88899-55-2
Critical Commercial Assays		
Mouse anti-human CD14 microbeads	Miltenyi Biotec	Cat# 130-050-201
LS magnetic columns	Miltenyi Biotec	Cat# 130-042-401
Protein G Agarose, Fast Flow	Millipore	Cat# 16-266
Renilla Luciferase Assay	Promega	Cat# E2810
Amersham ECL Prisme Western Blotting Detection Reagent	GE Healthcare	Cat# RPN2232
SuperSignal WestPico Chemiluminescent Substrate	Thermo Scientific	Cat# 34080
Matrigel	BD Bioscience	Cat# 356234
IL-10 ELISA set	BD Bioscience	Cat# 555157
Human CD163 ELISA kit	BD Bioscience	Cat# DY1607-05
Human Mer ELISA kit	BD Bioscience	Cat# DY6488
Human TruStain FcX	Biolegend	Cat#422302
Cell Dissociation Buffer	Thermo Fisher Scientific	Cat# 13151014
Phalloidin AlexaFluor 488	Thermo Fisher Scientific	Cat# A12379
DAPI	Sigma Aldrich	Cat# D9542
Vybrant® DiO	Thermo Fisher Scientific	Cat# V22886
CellTracker Red CMPTX Dye	Thermo Fisher Scientific	Cat# C34552
CellTracker Green CMFDA Dye	Thermo Fisher Scientific	Cat# C7025
Fluorescence Mounting Medium	Agilent Technologies	Cat# S302380-2
Prolong anti-fade reagent	Thermo Fisher Scientific	Cat# P10144
Experimental Models: Cell Lines		
TZM-bl cell line	NIH AIDS Reagent Program	Cat# 8129
Software and Algorithms		
ImageJ	ImageJ	https://www.imagej.nih.gov/ij/
Prism (v5)	GraphPad	https://www.graphpad.com/
Photoshop CS3	Adobe	https://www.adobe.com/
Illustrator CS3	Adobe	https://www.adobe.com/

(*Continued on next page*)

Continued

REAGENT or RESOURCE	SOURCE	IDENTIFIER
Huygens Professional Version 16.10	Scientific Volume Imaging	https://svi.nl/Huygens-Professional
FACS DIVA	BD Bioscience	http://www.bdbiosciences.com/
FlowJo 7.6.5	TreeStar	https://www.flowjo.com/
FCS Express V3	DeNovo Software	http://www.denovosoftware.com
Image Lab	Bio-Rad Laboratories	http://www.bio-rad.com

CONTACT FOR REAGENT AND RESOURCE SHARING

Further information and requests for reagents should be directed to and will be fulfilled by the Lead Contact, Geanncarlo Lugo-Vilarino (lugo@ipbs.fr). Sharing of antibodies and other reagents with academic researchers may require UBMTA agreements.

EXPERIMENTAL MODEL AND SUBJECT DETAILS

Human Subjects

Monocytes from healthy subjects (HS) were provided by Etablissement Français du Sang, Toulouse, France, under contract 21/PLER/TOU/IPBS01/20130042. According to articles L12434 and R124361 of the French Public Health Code, the contract was approved by the French Ministry of Science and Technology (agreement number AC 2009921). Written informed consents were obtained from the donors before sample collection. The sex of HS is unknown.

Tuberculous (TB) patients from the División de Tisioneumonología at the Instituto de Tisioneumonología Vaccarezza-University of Buenos Aires, Argentina and co-infected HIV/TB patients from the Division de SIDA at the Hospital F.J Muñiz, from 2015 to 2016, were diagnosed by the presence of recent clinical respiratory symptoms, abnormal chest radiography and positive sputum smear test for acid-fast bacilli. The research was carried out in accordance with the Declaration of Helsinki (2013) of the World Medical Association, and was approved by the Ethics Committees of the institutes mentioned above (protocol numbers: NIN-1671-12 and proceedings 37/38). Written informed consent was obtained before sample collection. Exclusion criteria included the presence of concurrent infectious diseases or non-infectious conditions (cancer, diabetes, or steroid therapy). Blood samples were collected at 3 to 10 days after start of TB treatment. The diagnosis of tuberculous pleurisy was based on a positive Ziehl–Nielsen stain or Lowestein–Jensen culture from pleural effusion (PE) and/or histopathology of pleural biopsy, and was further confirmed by an *Mycobacterium tuberculosis*-induced IFN-γ response and an ADA-positive test (Light, 2010). Effusions were classified as exudates according to Light (2010). PE and peripheral blood (PB) samples were obtained as described previously (Schierloh et al., 2007). PB samples from HS were provided by the Blood Transfusion Service, Hospital Fernandez, Buenos Aires (agreement number CEIANM-52-5-2012). All HS had received BCG vaccination in childhood and their tuberculin-test status (TTS) was unknown. Clinical features and sex of the experimental groups are summarized in Table S1.

Strategy for randomization and/or stratification

Blood samples from enrolled patients were classified in 3 groups of individuals: 1) TB patients with abnormal chest radiography and positive sputum smear test for acid-fast bacilli, who received less than one week of anti-TB therapy (TB); 2) HIV-1 infected patients with active TB, who received less than one week of anti-TB therapy (HIV/TB); and 3) Bacillus Calmette-Guerin-vaccinated healthy donors (HS). Pleural effusions samples from enrolled patients were classified in 2 groups of individuals: 1) TB pleurisy based on a positive Ziehl–Nielsen stain or Lowestein–Jensen culture from PE and/or histopathology of pleural biopsy, and confirmed by an Mtb-induced IFN-γ response and an adenosine deaminase-positive test; and 2) no-TB pleurisy including the following etiologies: malignant effusions (mesothelioma, lung carcinoma or metastatic patients), parapneumonic effusions and heart failure associated effusions.

Inclusion and Exclusion criteria for blood samples

Inclusion: *p*erson > 21 years old diagnosed with TB (clinical or laboratory criteria) having HIV^+ serology (HIV/TB) or not and who consent to participate. Exclusion: the presence of concurrent infectious diseases, except HIV, or non-infectious conditions (cancer, diabetes, or steroid therapy) and patients who do not provide consent.

Inclusion and Exclusion criteria for pleural effusion samples

Inclusion: person > 21 years old having a pleural effusion requiring drainage by therapeutic thoracentesis and who consent to participate. *Exclusion:* the presence of empyema, pleural effusion that does not require therapeutic drainage and patients who do not provide consent.

The GPower software was used for sample-size estimation and statistics. No replicates and no blinding were done.

NHPs

All animal procedures were approved by the Institutional Animal Care and Use Committee of Tulane University, New Orleans, LA, and were performed in strict accordance with NIH guidelines. The twenty adult rhesus macaques used in this study (Table S2) were bred

and housed at Tulane National Primate Research Center (TNPRC). The sex of animals is specified in Table S2. All macaques were infected as previously described (Foreman et al., 2016; Mehra et al., 2011). Briefly, macaques were aerosol-exposed to a low dose (25 CFU implanted) of Mtb CDC1551 and a subset of the macaques were also exposed 9 weeks later to 300 TCID50 of SIVmac239 administrated intravenously in 1mL saline. The control subset received an equal volume of saline intravenously. Criteria for killing included presentation of four or more of the following conditions: (i) body temperatures consistently greater than 2°F above preinfection values for 3 or more weeks in a row; (ii) 15% or more loss in body weight; (iii) serum CRP values higher than 10 mg/mL for 3 or more consecutive weeks, CRP being a marker for systemic inflammation that exhibits a high degree of correlation with active TB in macaques (Kaushal et al., 2012; Mehra et al., 2011); (iv) CXR values higher than 2 on a scale of 0–4; (v) respiratory discomfort leading to vocalization; (vi) significant or complete loss of appetite; and (vii) detectable bacilli in BAL samples.

Bacteria

Mtb H37Rv strain was grown in 7H9 media at 37°C, as described (Lastrucci et al., 2015). Exponentially growing Mtb was centrifuged (460 g) and resuspended in PBS ($MgCl_2$, $CaCl_2$ free, GIBCO). Clumps were dissociated by 20 passages through a 26-G needle then resuspended in RPMI-1640 containing 10% FBS. Bacterial concentration was determined by measuring OD_{600}.

Viruses

Proviral infectious clones of the macrophage-tropic HIV-1 isolate ADA (Vérollet et al., 2015a) was kindly provided by Serge Benichou (Institut Cochin, Paris, France). Virions were produced by transient transfection of 293T cells with proviral plasmids, as previously described (Vérollet et al., 2015a). HEK293 T cells (the sex of original cells is unknown) were maintained in DMEM, 20% FBS, 5% CO2. HIV-1 p24 antigen concentration of viral stocks was assessed by an home-made ELISA. HIV-1 infectious units were quantified, as reported (Vérollet et al., 2015a) using TZM-bl cells. TZM-bl cells are HeLa cell lines (female origin) that were obtained through NIH AIDS Reagent Program, Division of AIDS, NIAID, NIH from Dr. John C. Kappes, Dr. Xiaoyun Wu and Tranzyme Inc). In some experiments, we used Betalactamase (BlaM)-Vpr-containing ADA virus and NLAD8-VSVG pseudotyped viruses and HIV-1 ADA Gag-iGFP strain (see Key Resources Table).

Preparation of human monocytes and monocyte-derived macrophages

Monocytes from healthy subjects (HS) were isolated and differentiated into macrophages as previously described (Balboa et al., 2011; Lastrucci et al., 2015; Vérollet et al., 2015a). Briefly, purified $CD14^+$ monocytes from HS were differentiated for 5-7 days in RPMI-1640 medium (GIBCO), 10% Fetal Bovine Serum (FBS, Sigma-Aldrich) and human M-CSF (Peprotech) at 20 ng/mL. Differentiated macrophages were used as the cellular source to prepare the CmMTB after infection with Mtb. The cell medium was renewed every 3 or 4 days.

For the human samples of peripheral blood and pleural effusion (PE) from nonTB, TB and HIV/TB patients and HS, mononuclear cells were isolated by Ficoll-Hypaque gradient centrifugation (Pharmacia, Uppsala, Sweden), as described previously (Balboa et al., 2011; Lastrucci et al., 2015). Isolated monocytes from patients were allowed to adhere to 24-well plates, at $5x10^5$ cells/well for 1 h at 37°C in warm RPMI-1640 medium. The medium was then supplemented to a final concentration of 10% FBS and human recombinant M-CSF at 10 ng/mL. Flow cytometry analysis was performed in mononuclear cells, gating within the $CD14^+$ population.

METHODS DETAILS

Chemicals

When stated, monocytes (day 0) are treated with STAT3 activation inhibitor Stattic (1μM, kindly provided by Fabienne Meggetto from CRCT, INSERM Toulouse). In some conditions, monocytes (day 0) were treated with an inhibitor of TNT formation (TNTi, 20μM, Pharmeks), which was renewed after HIV-1 infection. In some experiments, macrophages were treated with Cytochalasin D (Sigma-Aldrich) at 2 μM. DMSO alone was used as vehicle control.

Preparation of conditioned media and cytokine depletion

The preparation of the conditioned medium of Mtb-infected macrophages (CmMTB) has been reported previously (Lastrucci et al., 2015). Briefly, macrophages were infected with Mtb H37Rv at a MOI of 3. The conditioned control medium (CmCTR) was obtained from uninfected macrophages. After incubation at 37°C for 18h, culture media were collected, sterilized by double filtration (0.2μm pores) and aliquots were stored at −80°C. For cytokine depletion experiments, CmCTR or CmMTB were incubated with 10 μg/mL of control IgG or neutralizing IL-10 antibody (JES3-19F1, Biolegend) for 1h at 4°C. Afterwards, 50 μg/mL of 50% slurry Protein G agarose beads (EMD Millipore) were added and incubated for 1h at 4°C. Conditioned media were centrifuged (300 g) to remove antibody-bead complexes and then filtered (0.2 μm pores) before use. The depletion was controlled by ELISA.

Conditioning of monocytes with the secretome of Mtb-infected macrophages or pleural effusions from TB patients

Freshly isolated $CD14^+$ monocytes from HS were allowed to adhere in the absence of serum (4×10^5cells/24-well in 500μL or 2×10^6 cells/6-well in 1.5mL). After 1h of culture, 80% CmMTB or CmCTR supplemented with 20 ng/mL M-CSF and 20% FBS were added to the cells (vol/vol). For experiments with PE, samples were collected in heparin tubes and centrifuged at 300 g for 10 minutes at room

temperature without brake. The cell-free supernatant was transferred into new plastic tubes, further centrifuged at 12000 g for 10 minutes and aliquots were stored at −80°C. After having the diagnosis of the PE, pools were prepared by mixing same amounts of individual PE associated to a specific etiology. The pools were de-complemented at 56°C for 30 minutes, and filtered by 0.22 μm in order to remove any remaining debris or residual bacteria. Particularly, we studied 21 patients with PE that were divided according their etiology. First group had 8 patients with tuberculous PE (PE-TB), second group had 8 patients with parapneumonic PE (PE-NPI), and third group had 5 patients with transudates secondary to heart failure (PE-HF). PE-TB or PE-nonTB (PE-NPI and PE-HF) supplemented with 40ng/mL M-CSF and 40% FBS were added to the cells (25% vol/vol). Cells were then cultured for 3 days. Monocytes were also conditioned in presence of 10 ng/mL M-CSF and 10 ng/mL recombinant human Interleukin-10 (IL-10) (PeproTech). Cell-surface expression of macrophage activation markers was measured by flow cytometry using standard procedures detailed in Star Methods.

HIV-1 infection of cells

Cells were infected with HIV-1 ADA strain at day 3 of culture at MOI 0.1. HIV-1 infection and replication were assessed 10 days post-infection by measuring p24-positive cells by immunostaining and the level of p24 released in culture media by ELISA.

Blam-Vpr fusion assay

Experiments were carried out as described previously (Garcia-Perez et al., 2015). Briefly, monocytes adhered on glass coverslips were conditioned for 3 days with CmMTB or CmCTR medium and then collected with cell dissociation buffer (Thermo Fisher Scientific). Then, 1.5×10^5 cells were incubated for 3 h at 37°C with 100 ng p24 of a Betalactamase (BlaM)-vpr-containing ADA virus. Infected cells were next incubated for 2 h with the CCF2/AM dye according to the manufacturer's instructions (Invitrogen). After washing, cells were fixed in 2% paraformaldehyde. Enzymatic cleavage of CCF2 by BlaM, which causes a blue-shift in the CCF2 fluorescence emission spectrum, was measured by flow cytometry (FACSCanto, BD Biosciences).

Flow cytometry

Staining of conditioned monocytes-to-macrophage population was performed as previously described (Lastrucci et al., 2015). Adherent cells were harvested using Cell Dissociation Buffer (Life Technologies), centrifuged for 5 min at 340 *g*, incubated in staining buffer (PBS, 2mM EDTA, 0.5% FBS) with a 1:100 dilution of Human TruStain FcX (Biolegend) for 5 minutes at room temperature. Cells were then stained in cold staining buffer for 25 min with fluorophore-conjugated antibodies (see Key Resources Table) and, in parallel, with the corresponding isotype control antibody using a general dilution of 1:400. After staining, the cells were washed with cold staining buffer, centrifuged for 5 min at 340*g* at 4°C (twice), and analyzed by flow cytometry using LSR-II flow cytometer (BD Biosciences) and the associated BD FACSDiva software. Data was then analyzed using the FlowJo 7.6.5 software (TreeStar). The monocyte-to-macrophage population was first gated according to its Forward Scatter (FSC) and Size Scatter (SSC) properties before singlet selection and analysis of the percentage of positive cells and the median fluorescence intensity (MFI) for each staining.

Cells from nonTB, TB and HIV/TB patients and related controls from HS (2×10^5 cells) were labeled as described above and acquired in a FACSAria II cytometer (BD Biosciences) and analyzed using FCS Express V3 software (*De Novo* Software, Los Angeles, CA, USA).

Immunofluorescence microscopy

Cells were fixed with PFA 3.7%, Sucrose 30mM in PBS. Stainings were performed as described (Vérollet et al., 2015a). Briefly, cells were permeabilized with Triton X-100 0.3% for 10 minutes, and saturated with PBS BSA 1% for 30 minutes. Cells were incubated with anti-Gag KC57 antibody (1:100, Beckman Coulter) in PBS BSA 1% for 1 hour, washed and then incubated with Alexa Fluor 555 Goat anti-Mouse IgG secondary antibody (1:1000, Cell Signaling Technology), Alexa Fluor 488 Phalloidin (1:500, Thermo Fisher Scientific) and DAPI (500 ng/mL, Sigma Aldrich) in PBS BSA 1% for 30 minutes. Coverslips were mounted on a glass slide using Fluorescence Mounting Medium (Dako). Slides were visualized with a Leica DM-RB fluorescence microscope or a FV1000 confocal microscope (Olympus). For deconvolution images shown in Figures 5E, S5A, and S5C, macrophages were imaged over nine planes at 100 nm intervals with a 100x/1.49 Nikon objective mounted on a Nikon Eclipse Ti-E and an Hamamatsu Orca flash 4.0 LT sCMOS. All images were deconvolved with Huygens Professional version 16.10 (Scientific Volume Imaging, the Netherlands), using the CMLE algorithm, with SNR:20 and 40 iterations.

For the deconvolution image shown in Figure 7D, imaging was performed using a dragonfly multimodal imaging platform in three-dimensional fast confocal mode using a 63x/1.47 objective and a Zyla 4.2 PLUS sCMOS camera (Andor).

TNTs were detected and counted using Phalloidin and microtubules staining. We quantified both thick and thin nanotubes: thin membrane nanotubes contained only F-actin, whereas thick TNTs contained both F-actin and microtubules.

As HIV-1 infection of macrophages makes them fuse into MGCs (Orenstein, 2001; Vérollet et al., 2010), the number of infected cells largely underestimates the rate of infection. Thus, to better reflect the rate of infection, we quantified HIV infection index (HIV-stained area divided by total cell area x 100), percentage of nuclei in multinucleated cells and percentage of multinucleated cells. These parameters were assessed by using semi-automatic quantification with home-made ImageJ macros, allowing the study of more than 5,000 cells per condition in at least five independent donors.

HIV-1 and DiO transfer monitoring

Freshly isolated $CD14^+$ monocytes from HS were allowed to adhere in the absence of serum (2×10^6 cells/6-well in 1.5mL). After 1h of culture, RPMI medium supplemented with 20 ng/mL M-CSF and 20% FBS and 20ng/mL IL-10 were added to the cells (vol/vol). At day 3, half cells are infected with 120ng p24 of a HIV-1 NLAD8 strain pseudotyped with a VSVG envelope. The other half cells are stained with CellTracker Green CMFDA Dye at day 5 (Thermo Fisher Scientific). Briefly, cells are washed with Mg^{2+}/Ca^{2+}-containing PBS and stained for 30 minutes in Mg^{2+}/Ca^{2+}-containing PBS supplemented with 500 ng/mL CellTracker, then washed with FBS-containing RPMI medium. HIV^+ and $CellTracker^+$ were then detached using accutase and co-cultured at a 1:1 ratio. In order to co-culture HIV^+ and $CellTracker^+$ cells in conditions that allow their physical separation, HIV^+ cells were plated on 6.5-mm transwell filters with 0.4 μm pore polyester membrane insert (Sigma-Aldrich) while $CellTracker^+$ cells were plated on coverslips at the bottom of 24-well plates holding the transwell filters. The cells therefore shared only the culture medium but were unable to physically contact each other. For the cell-free HIV-1 control, $CellTracker^+$ cells were incubated with the supernatant of HIV^+ cells containing produced virions. After 24 h, cells were fixed, stained and imaged.

For DiO transfer monitoring, cells were stained either with CellTracker Red CMPTX Dye (Thermo Fisher Scientific) as described above, or with a lypophylic tracer Vybrant® DiO (Thermo Fisher Scientific), according to manufacturer's instructions. Then, cells were detached using accutase, co-cultured at a 1:1 ratio in 8-well Lab-Tek® chambers for 24h and imaged.

Scanning electron microscopy

Scanning electron microscopy observations were performed as previously described (Lastrucci et al., 2015). Briefly, HIV-1-infected macrophages were fixed in 2.5% glutaraldehyde/3.7% PFA/0.1M sodium cacodylate (pH 7.4), post-fixed in 1% osmium tetraoxide (in 0.2M cacodylate buffer), dehydrated in a series of increasing ethanol. Critical point was dried using carbon dioxide in a Leica EMCPD300. After coating with gold, cells were examined with a FEI Quanta FEG250 scanning electron microscope.

Immunoblot analyses

Total protein lysates were extracted as previously described (Lastrucci et al., 2015; Vérollet et al., 2015a). Total proteins were separated through SDS-polyacrylamide gel electrophoresis, transferred and immunoblotted overnight at 4°C with indicated primary antibodies (See Key Resources Table). Secondary antibodies were the following: Anti-rabbit and anti-mouse IgG, HRP-linked Antibody (Cell Signaling Technology). Proteins were visualized with Amersham ECL Prime Western Blotting Detection Reagent (GE Healthcare). Chemiluminescence was detected with ChemiDoc Touch Imaging System (Bio-Rad Laboratories) and quantified using Image Lab software (Bio-Rad Laboratories).

For the detection of LC3 autophagy protein, monocytes were seeded on 12-well plates at a density of 0.8×10^6 cells by well. After infection and treatment with Bafilomycin A1 (100 nM) or DMSO vehicle control for 2 h, cells were lysed. Proteins harvested were subjected to a SDS-polyacrylamide gel electrophoresis, 4%–15% gradient (Biorad). Blots were blocked with 5% dried milk in PBS, incubated with LC3 primary antibody and then with the corresponding horseradish peroxidase-conjugated secondary antibody (ThermoScientific). Staining was detected with SuperSignal WestPico Chemiluminescent Substrate (ThermoScientific), and immunostained proteins were visualized using the ChemidocTouch Imaging System (Biorad). Densitometric LC3-II/actin ratios were measured using the ImageJ software.

3D migration assays

3D migration assays of cells in Matrigel (10–12 mg/mL, BD Biosciences) were performed as described (Vérollet et al., 2015a) and quantified at 48h. Briefly, pictures of cells were taken automatically with a 10X objective at constant intervals using the motorized stage of an inverted microscope (Leica DMIRB, Leica Microsystems). Cells were counted using ImageJ software as described previously (Vérollet et al., 2015a). The number of cells inside the matrix (% of migration measured after 48h of migration) was quantified.

Protein quantifications in cell-free fluids by ELISA

Soluble protein concentration was measured in cell supernatants by ELISA using kits from BD Bioscience (IL-10) and R&D Systems (sCD163 and sMer), according to manufacturer's instructions.

Cytotoxicity assay

To exclude any impact of cytotoxicity of TNTi used in this study we measured lactate dehydrogenase (LDH) activity released from the cytosol of damaged cells into the supernatant. LDH release was measured using the Cytotoxicity Detection kit (Roche, Mannheim, Germany) according to the manufacturer's instructions. Monocytes were treated with TNTi (20μM) or DMSO as a control for 13 days. Cell-free culture supernatants were collected and incubated with LDH assay solution at 25°C for 30 min. The optical density values were analyzed at 490 nm by subtracting the reference value at 620 nm.

Phagocytosis assay

IgG-opsonized zymosan was prepared by incubating particles in suspension in PBS with human IgG (13 mg/mL, 30 min at 37°C) and washing as described (Le Cabec and Maridonneau-Parini, 1994). The number of particles was counted in a Malassez chamber. FITC-labeled zymosan particles were then added at a MOI of 5 and incubated for 30 minutes at 37°C. Cells were then extensively washed

with PBS and fixed in 3.7% PFA. To exclusively quantify phagocytosis and not binding, extracellular zymosan was stained as described (Le Cabec et al., 2000).

Histological analyses

Paraffin embedded tissue samples were sectioned and stained with hematoxylin and eosin for histomorphological analysis. Immunohistochemical staining was performed on paraffin-embedded tissue sections, using anti-CD163 (10D6, mouse mAb, Leica/Novocastra) and anti-pSTAT3 (D3A7 rabbit mAb, Cell Signaling Technology). Immunostaining of paraffin sections was preceded by different antigen unmasking methods. After incubation with primary antibodies, sections were incubated with biotin-conjugated polyclonal anti-mouse or anti-rabbit immunoglobulin antibodies followed by the streptavidin-biotin-peroxidase complex (ABC) method (Vector Laboratories) and then were counter-stained with hematoxylin. Slides were scanned with the Panoramic 250 Flash II (3DHISTECH). Virtual slides were automatically quantified for macrophage distribution as previously described (Lastrucci et al., 2015; Vérollet et al., 2015a). For confocal microscopy, samples were stained with primary antibodies as described above and followed by anti-mouse IgG isotype specific or anti-rabbit IgG antibodies labeled with Alexa488 and Alexa555 (Molecular Probes). Samples were mounted with Prolong® Antifade reagent (Molecular Probes) and examined using a 60x/1.40N.A. objective of an Olympus FV1000 confocal microscope.

QUANTIFICATION AND STATISTICAL ANALYSIS

Information on the statistical tests used, and the exact values of n (number of donors) can be found in the Figure Legends. All statistical analyses were performed using GraphPad Prism 6.0 (GraphPad Software Inc.). The statistical tests were chosen according to the following. Two-tailed paired or unpaired t test was applied on datasets with a normal distribution (determined using Kolmogorov-Smirnov test), whereas two-tailed Mann-Whitney (unpaired test) or Wilcoxon matched-paired signed rank tests were used otherwise. $p < 0.05$ was considered as the level of statistical significance (* $p \leq 0.05$; ** $p \leq 0.005$; *** $p \leq 0.0005$; **** $p \leq 0.0001$).